communications biology

A Nature Portfolio journal

Article

https://doi.org/10.1038/s42003-025-08878-z

SIRT5-mediated desuccinylation of MTHFD2 enhances chemoresistance in breast cancer cells by reducing therapy-induced senescence

Zhang Xianhong[1,3], Gao Yue[1,3], Zhang Yu[1], Zhang Yichen[1], Chen Yufei[1], Pei Xinke[1], Zhang Jinhui[1], Wang Yiqi[1], Du Yitian[1] ✉, Hao Shuailin[1] ✉ & Ni Ting[1,2] ✉

Protein lysine succinylation is a crucial post-translational modification that regulates nearly all aspects of eukaryotic and prokaryotic cell, including gene transcription, cell metabolism and redox homeostasis. Among them, metabolic disorders caused by dysfunctional post-translational modifications induce aging and aged-related diseases, including cancer. This study quantified the dynamic changes in protein succinylation in response to DNA damage stress induced by etoposide (ETOP) in tumor cells. A total of 4354 lysine succinylation sites on 1259 proteins were identified, many of which have not been previously reported. Bioinformatics analysis revealed that many proteins are involved in the metabolism of nicotinamide adenine dinucleotide phosphate (NADPH) in mitochondria (including MTHFD2). We further found that low activity or depletion of MTHFD2 enhances the degree of TIS in breast cancer cells and decreases their resistance to chemotherapeutic agents. Interestingly, we also found that SIRT5-mediated desuccinylation of MTHFD2 was able to reduce the senescence of breast cancer cells, thereby enhancing their resistance to chemotherapeutic drugs. This effect may explain the poorer prognosis observed in breast cancer patients with high expression levels of SIRT5 or MTHFD2. These systematic analyses provide new insights into targeting succinylation-modified metabolic proteins to enhance TIS, and their combination with senolytics for breast cancer therapy.

Breast cancer is now the most commonly diagnosed cancer in the world[1]. Although the regular treatment options including surgery, radiotherapy, and chemotherapy are well established, most chemotherapeutic agents lack efficacy in the treatment of metastatic breast cancer due to the development of drug resistance[2,3]. It is worth noting that "non-lethal dose chemotherapy" is a new type of chemotherapy, which has the advantages of less toxic side effects, significantly improved patient tolerance and better efficacy. It has been found that the morphology and metabolic activity of cells treated with "non-lethal dose chemotherapy" undergo important changes, and tends to "choose" to enter the state of senescence[4]. Indeed, classical chemotherapeutic agents including etoposide (ETOP), Doxorubicin, Olaparib, Cisplatin, and Bleomycin are a viable and effective form of cancer treatment that can be administered alone or in combination with surgery or radiotherapy. These chemotherapeutic agents can induce transformed breast cancer cells to enter a similar state of senescence, also known as therapy-induced tumor cell senescence (TIS), by inducing DNA damage-associated genotoxic stress and high levels of reactive oxygen species (ROS)[5,6]. Notably, TIS combined with senolytics, small molecules that selectively eliminate senescent cells, has recently emerged as a novel strategy in breast cancer therapy. Compared with the traditional method of killing tumor cells directly with drugs, this "combo" strategy is more specific and effective for certain tumor cells with specific genetic backgrounds[7]. Unfortunately, breast cancer cells will avoid the ROS threshold of cellular senescence through a strong metabolic reprogramming ability and antioxidant defense

[1]State Key Laboratory of Reproductive Regulation and Breeding of Grassland Livestock, Institutes of Biomedical Sciences, School of Life Sciences, Inner Mongolia University, 010070 Hohhot, P.R. China. [2]State Key Laboratory of Genetics and Development of Complex Phenotypes, National Clinical Research Center for Aging and Medicine, Huashan Hospital, Collaborative Innovation Center of Genetics and Development, Human Phenome Institute, Center for Evolutionary Biology, Shanghai Engineering Research Center of Industrial Microorganisms, School of Life Sciences, Fudan University, 200438 Shanghai, P.R. China. [3]These authors contributed equally: Zhang Xianhong, Gao Yue. ✉e-mail: yitian_du@163.com; shuailh@imu.edu.cn; tingni@fudan.edu.cn

mechanisms, thus enhancing resistance to chemotherapeutic agents. These findings suggest that the adaptation of breast cancer cells to oxidative stress is essential for the maintenance of drug resistance. Therefore, exploring metabolic targets to enhance TIS and reduce the resistance of breast cancer cells to chemotherapeutic drugs is a critical step for early tumor treatment.

Protein post-translational modifications (PTMs) are widespread molecular mechanisms that regulate chromatin dynamics and gene expression[8]. Phosphorylation and acetylation are among the most extensively studied PTMs, whereas succinylation has only recently been recognized as a novel PTM. Succinylation involves the covalent attachment of a succinyl group to the epsilon-amino group of lysine residues, thereby altering the function of substrate proteins[9]. Increasing evidence indicates that succinylation modulates the activity of metabolic enzymes and reprograms metabolic pathways in cancer cells particularly mitochondrial metabolism including the tricarboxylic acid (TCA) cycle, electron transport chain, glycolysis, fatty acid oxidation, and the urea cycle[10–14]. More importantly, succinylation can also promote tumor progression by regulating cancer-associated proteins[15,16]. However, studies on the role of succinylation in breast cancer remain limited. SIRT5, the primary desuccinylase, catalyzes NAD^+-dependent desuccinylation and is predominantly localized in the mitochondrial matrix[17]. Early studies have implicated SIRT5 in cellular senescence, cancer progression, and antioxidant defense[18–21]. Although SIRT5 has been reported to be highly expressed in human breast cancer and correlated with poor patient prognosis[22], its functional role in regulating breast cancer cell proliferation and chemoresistance remains largely unknown.

Mitochondria-mediated metabolic reprogramming plays a pivotal role in cancer progression[23]. Mitochondrial methylenetetrahydrofolate dehydrogenase (MTHFD2) is a key enzyme in the mitochondrial one-carbon (1C) metabolism pathway and contributes to the production of nicotinamide adenine dinucleotide phosphate (NADPH), which is involved in maintaining redox homeostasis[24]. Reduction or loss of MTHFD2 has been associated with metabolic stress and mitochondrial-related dysfunction[25]. Indeed, mitochondrial metabolism is able to provide succinyl-CoA and NADPH for rapid tumor cell proliferation, succinyl-CoA serves as a critical substrate for succinylation modification of the lysine moiety of proteins, whereas NADPH is essential for maintaining ROS homeostasis in tumor cells[26,27]. ROS produced by excessive proliferation of tumor cells are toxic[28]. Thus, tumor cells activate powerful antioxidant defense mechanisms to avoid ROS thresholds that trigger cellular senescence, apoptosis, or iron death[29]. This powerful antioxidant mechanism relies on the intracellular production of the antioxidant reducing substance NADPH[30]. Previous studies have shown that breast cancer cells, compared to non-malignant cells, often sustain elevated levels of NADPH. This not only fuels antioxidant defenses but also enables the metabolic plasticity required for metastasis[31]. The aberrant overexpression of NADPH-generating enzymes, such as MTHFD2, is a common feature of various cancers and is closely linked to unfavorable patient prognosis[32–34]. However, the regulation of MTHFD2 succinylation and its potential role in mediating chemoresistance in breast cancer remain poorly understood.

Oncogene-induced senescence (OIS) and TIS are well-established tumor-suppressive mechanisms[35]. However, the mechanisms by which breast cancer cells evade senescence triggered by various stressors, such as DNA damage, oncogenic signaling, ROS, and genotoxic stress induced by cancer therapies, remain poorly understood. Recent studies have found that acetylation or lactylation modifications of histones and non-histone proteins in tumor cells lead to chemotherapy resistance in tumor cells[36–38]. In contrast, the role of protein succinylation in mediating drug resistance in breast cancer has received relatively little attention. Mitochondrial metabolites, notably succinyl-CoA and NADPH, play essential roles in regulating protein succinylation and preserving intracellular ROS homeostasis[38]. The succinylation status of mitochondrial NADPH-generating enzymes and their potential role in regulating senescence and chemoresistance in breast cancer have yet to be elucidated. This motivates us to explore metabolic targets that reduce chemoresistance in breast cancer cells and to search for effective ways to induce cellular senescence and block breast cancer cell proliferation. In this study, we investigated the overall dynamics of protein lysine succinylation in tumor cells after ETOP treatment. It was found that succinylation modifications occurring at the lysine (K44) site decrease the activity of MTHFD2. This modification facilitates breast cancer cells' entry into TIS, thereby reducing their resistance to chemotherapeutic agents. In contrast, SIRT5-mediated desuccinylation of MTHFD2 reduces cellular senescence and further enhances chemoresistance in breast cancer cells. Our results suggest that succinylated MTHFD2 is a metabolic target to enhance TIS, and depletion of MTHFD2 in combination with senolytics is a strategy to increase sensitivity to chemotherapeutic agents in breast cancer.

Results

Lysine succinylated (Ksuc) proteins are mainly enriched in cellular metabolic processes after ETOP treatment

Since aberrant regulation of lysine succinylation occurs in different cancers, inhibitors targeting lysine succinylation-regulating enzymes are often used as potential anticancer strategies[39]. Although many experiments have shown that lysine succinylation can regulate tumor cell growth and metastasis by modulating protein stability and function, it is also associated with the DNA damage response (DDR) and immunity[40]. However, it is not clear whether lysine succinylation is involved in and regulates chemoresistance in tumor cells. To explore the dynamics of lysine succinylated proteins in tumor cells in response to chemotherapeutic agents and to search for lysine succinylated proteins that may reduce chemoresistance. U2OS cells were treated with 20 μM ETOP for 24 h, then digested and lysed. The proteins were subsequently purified using anti-succinylated lysine antibodies. The samples were then analyzed using high-resolution liquid chromatography-tandem mass spectrometry (LC-MS/MS) (Fig. 1A).

The results showed that the MS data identified 4,354 lysine succinylation sites across 1259 proteins, of which 4086 sites were quantified for 1175 proteins (Fig. 1B). Based on the differential analysis, a P-value < 0.05 with a change in differential expression exceeding 1.5 was considered a significant upregulation threshold, while a change level less than 1/1.5 was considered a significant downregulation threshold. Accordingly, 744 lysine succinylation sites were identified as upregulated, while 242 sites were identified as downregulated (Fig. 1C). To further determine the functions of these succinylated proteins, we classified the upregulated and downregulated proteins based on their subcellular locations. Among the identified upregulated succinylated proteins, 33.6% were located in the cytoplasm, 40.8% in the mitochondria, and 9.4% in the nucleus. Among the downregulated succinylated proteins, 48% were located in the cytoplasm, 9.8% in the mitochondria, and 32.4% in the nucleus (Fig. 1D). These results indicate that many succinylation-modified proteins are upregulated in cells following ETOP-induced DNA damage, suggesting the complexity of these modifications and the relatively independent functions of succinylated proteins. In order to elucidate the potential roles of lysine succinylated proteins in response to ETOP treatment, all identified differentially succinylated proteins were subjected to COG/KOG classification, which showed that these differentially expressed proteins are mainly involved in intracellular signal transduction, genetic information storage and metabolic processe (Fig. 1E). Notably, KEGG functional enrichment analysis revealed that the top 20 most significantly enriched functions among these differentially succinylated proteins included pyruvate metabolism, the TCA cycle, and glycogen allosteric regulation (Fig. 1F). This suggests that Ksuc proteins are most enriched in cellular metabolism in U2OS cells following ETOP treatment.

Notably, among the identified upregulated succinylated proteins, 40.8% in the mitochondria (Fig. 1D). Mitochondria were found to support tumor cell anabolism by providing key metabolites for macromolecular synthesis and producing tumor metabolites to maintain cancer phenotypes[41]. As mentioned previously, mitochondrial metabolism-derived succinyl coenzyme A and NADPH are important metabolites for cells to undergo succinylation modifications and maintain ROS homeostasis. Since LC/MS data showed that differentially succinylated proteins after ETOP treatment have a distribution in mitochondria and are functionally enriched

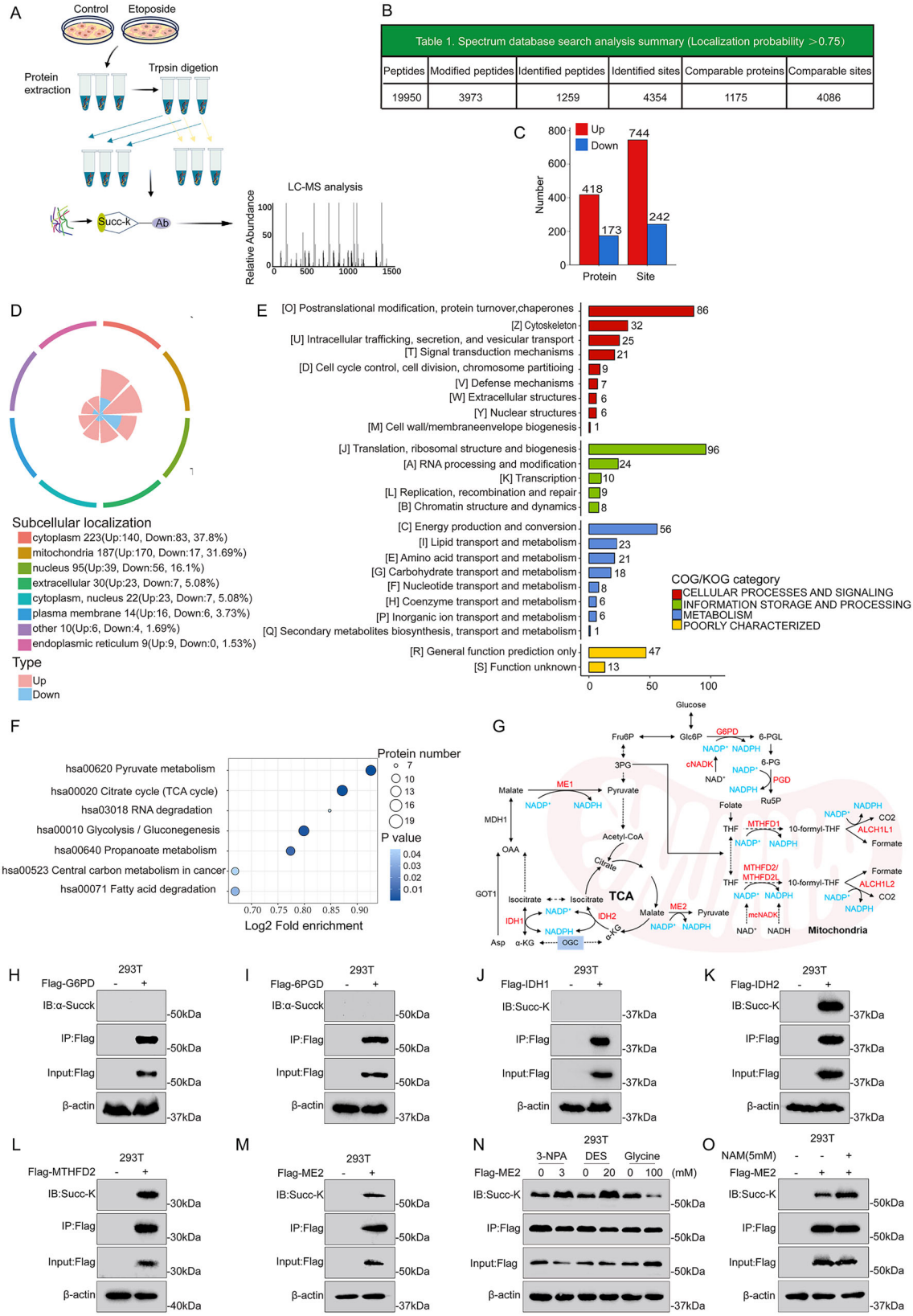

mainly for cellular metabolic processes. Therefore, we focused on changes in succinylation located within the mitochondria and capable of producing NADPH metabolizing enzymes. NADPH steady-state is maintained by the regulation of various metabolic pathways and enzymes, including NAD kinase (NADK), the pentose phosphate pathway (PPP), carbon metabolism, malic acid, malic enzyme (ME), nicotinamide nucleotide transhydrogenase (NNT), and cytoplasmic or mitochondrial NADP-dependent isocitrate dehydrogenase (IDH1 and IDH2), as well as glutamine metabolism and fatty acid oxidation (FAO) (Fig. 1G). Alongside the succinylation-modified proteins identified by LC-MS following ETOP treatment of U2OS cells, we

Fig. 1 | Quantification and annotation of intracellular proteins and their succinylation in U2OS cells treated with ETOP. A Schematic diagram of the quantitative proteomics analysis workflow for succinylation modification in U2OS cells after 24-hour treatment with 20 μM Etoposide. **B** LC-MS identification of the total number of peptides and the total number of loci. **C** Statistical analysis of differentially modified sites after treatment of U2OS cells with 20 μM of Etoposide. **D** The subcellular localization classification map was performed for the screened differential proteins. **E** After 20 μM Etoposide processing U2OS enrichment of COG/KOG on differences in modified protein function analysis. **F** Functional enrichment analysis of differentially modified proteins. KEGG pathway were included. **G** Mainly in the cell of NADPH metabolic pathways. **H**–**M** Pan-succinylated lysine antibody using western blotting. Succinylation levels of G6PD, 6PGD, IDH1, IDH2, MTHFD2, ME2-Flag ectopically expressed in HEK293T cells were measured by the pan-succinylated lysine antibody. **N** Succinylation levels of ectopically expressed ME2 in HEK293T cells were measured. Cells were treated with 3-NPA (3 mM), DES (20 mM) or Glycine (100 mM) were used to treat cells for 24 h. **O** Succinylation levels of ectopically expressed ME2 in HEK293T cells were measured. Cells were treated with 5 mM NAM for 3 h before harvesting. ME2-Flag was immunoprecipitated from cell lysates and its succinylation was examined with a pan-succinylated lysine antibody.

specifically examined the succinylation levels of NADPH-metabolizing enzymes, including G6PD, 6PGD, MTHFD2, ME2, and IDH1/2. The results revealed that G6PD, 6PGD, and IDH1 did not exhibit succinylation modifications (Fig. 1H-J), while MTHFD2, IDH2, and ME2 did (Fig. 1K–M). Previous studies have shown that desuccinylated IDH2 promotes cancer cell growth by enhancing antioxidant defenses[42], while desuccinylated ME2 supports cancer growth by boosting mitochondrial respiration[43]. In this study, we focused on verifying the succinylation of ME2. As a central metabolite in the TCA cycle, succinyl-CoA acts as the principal donor of succinyl groups required for lysine succinylation. Its production is mainly derived from the metabolic conversion of α-ketoglutarate (α-KG) and succinate, linking mitochondrial metabolism to the regulation of post-translational modifications (Supplementary Fig. 1A). The irreversible SDH inhibitor 3-nitropropionic acid (3-NPA), which covalently binds to an arginine residue in the catalytic core of succinate dehydrogenase A (SDHA) to inactivate SDH, resulted in intracellular succinate accumulation[44]. Treatment of 293 T cells with 3 mM 3-NPA markedly elevated the succinylation level of ME2 (Fig. 1N). Similarly, exposure to 20 mM diethyl succinate (DES), a cell-permeable succinate analog, also increased ME2 succinylation (Fig. 1N). Conversely, glycine has been reported to reduce intracellular succinyl-CoA levels through its involvement in the heme biosynthesis pathway[45]. Treatment with 100 mM glycine significantly decreased the succinylation level of ME2 (Fig. 1N). Consistent with existing literature, we found that treating these cells with succinyl-CoA increased the succinylation levels of ME2 (Supplementary Fig. 1B), and treatment with the pan-sirtuin inhibitor nicotinamide (NAM) significantly enhanced ME2 succinylation levels (Fig. 1O). These findings confirm the presence of ME2 succinylation and validate the reliability of the LC-MS data. In addition to 293 T cells, where MTHFD2 was found to undergo succinylation (Fig. 1L), we also detected succinylation of MTHFD2 in multiple breast cancer cell lines, including MDA-MB-231, MDA-MB-468, and MCF-7 (Supplementary Fig. 1C–E). These findings indicate that MTHFD2 succinylation is not restricted to a specific cell type, but rather represents a conserved post-translational modification across diverse breast cancer subtypes, suggesting its potential functional relevance in tumor metabolism and progression.

SIRT5 activates MTHFD2 activity and promotes NADPH production through desuccinylation

Besides IDH2 and ME2, the succinylation modification of MTHFD2 has not been previously reported. LC-MS data revealed that succinylated MTHFD2 was upregulated after ETOP treatment, suggesting dynamic changes in MTHFD2 succinylation following ETOP-induced DNA damage (Fig. 2A). We have previously confirmed MTHFD2 succinylation through CO-IP experiments (Fig. 1L), and in vitro succinylation assays with varying amounts of succinyl-CoA showed dose-dependent increases in MTHFD2 succinylation levels (Fig. 2B). Consistently, treatment with 3 mM 3-NPA or 10 mM dimethyl α-ketoglutarate (DMK), a cell-permeable analog of α-ketoglutarate, led to a marked increase in the succinylation level of MTHFD2 in MDA-MB-231 cells. In contrast, exposure to 100 mM glycine significantly reduced MTHFD2 succinylation (Supplementary Fig. 2A). This further supports the existence of MTHFD2 succinylation modifications. To pinpoint potential succinylation sites on MTHFD2, we purified succinylated MTHFD2 protein from HEK293T cells and identified the sites using mass spectrometry, four potential succinylated lysine sites on MTHFD2-K44, K50, K88, and K286-were identified (Fig. 2C). We then created Arg (R) substitution mutants at eight adjacent lysine sites (K44, K50, K88, K93, K139, K164, K220, and K286) between lysines K44 and K286 to mimic the desuccinylated state and expressed these Flag-tagged MTHFD2 mutants in HEK293T cells. Among these mutants, the K44R mutant exhibited significantly lower succinylation levels, indicating that K44 is a critical succinylation site on MTHFD2 (Fig. 2D). LC-MS data also confirmed succinylation at K44 of MTHFD2 (Fig. 2E). These findings suggest that MTHFD2 is succinylated specifically at lysine K44.

In search of the desuccinylase of MTHFD2, we overexpressed Flag-tagged MTHFD2 in HEK293T and MDA-MB-231 cells, and treated them with the pan-sirtuin inhibitor NAM to inhibit SIRT desuccinylase activity. We confirmed that MTHFD2 was succinylated and that NAM treatment increased its succinylation levels (Fig. 2F, Supplementary Fig. 2B). We aimed to identify which SIRT enzyme mediates MTHFD2 desuccinylation. Initially, we conducted co-immunoprecipitation (co-IP) experiments with MTHFD2 and various SIRT members, including SIRT1-7. We discovered that only SIRT5 had significant desuccinylation effects on MTHFD2, with other sirtuins (SIRTs) showing no such effects (Fig. 2G). These results suggest that SIRT5 may be responsible for the desuccinylation of MTHFD2. To further validate the regulatory role of SIRT5 in MTHFD2 succinylation, we performed co-IP assays in HEK293T, MDA-MB-231, and MDA-MB-468 cells, and observed a physical interaction between SIRT5 and MTHFD2 (Fig. 2H, Supplementary Fig. 2C, D). Moreover, SIRT5 knockdown in MDA-MB-231, MDA-MB-468, and MCF-7 cells led to a marked increase in the succinylation level of MTHFD2 (Fig. 2I, Supplementary Fig. 2E, F). Conversely, MTHFD2 succinylation levels were significantly reduced upon SIRT5 overexpression in HEK293T cells (Fig. 2J). Furthermore, the SIRT5 N-terminal deletion mutant SIRT5Δ50, which cannot enter the mitochondria, failed to desuccinylate MTHFD2 (Fig. 2K). Similarly, the enzymatically defective SIRT5 mutant SIRT5-H158Y (histidine to tyrosine mutation) could not desuccinylate MTHFD2 (Fig. 2L). These findings suggest that SIRT5 is responsible for the desuccinylation of MTHFD2.

MTHFD2 is an active enzyme in one-carbon (1C) metabolism[46]. As we previously mentioned, MTHFD2 is succinylated at lysine K44, a conserved site across different species (Fig. 2M). Thus, we hypothesize that succinylation at the conserved site K44 may impact MTHFD2 enzymatic activity. To further investigate how succinylation at the K44 site affects MTHFD2 enzymatic activity. Cells treated with succinyl-CoA, which increased MTHFD2 succinylation levels, exhibited reduced MTHFD2 activity (Fig. 2N). Additionally, knockdown of SIRT5 in MDA-MB-231 cells led to increased MTHFD2 succinylation levels and reduced MTHFD2 activity (Fig. 2O). These findings suggest that MTHFD2 enzymatic activity is negatively correlated with its succinylation level, which is regulated by SIRT5. Given that K44 is a key succinylation site on MTHFD2, we further assessed whether K44 succinylation affects MTHFD2 enzymatic activity. We created Arg (**R**) and Glu (**E**) mutants to mimic desuccinylated and negatively charged succinyllysine states, respectively, and expressed FLAG-tagged WT MTHFD2 or MTHFD2 mutants (K44R, K44E) in HEK293T cells. We then performed immunoprecipitation and MTHFD2 enzymatic activity assays. MTHFD2 K44R activity did not change significantly, whereas the K44E mutant activity was markedly reduced compared to WT MTHFD2 (Fig. 2P). These data suggest that succinylation at

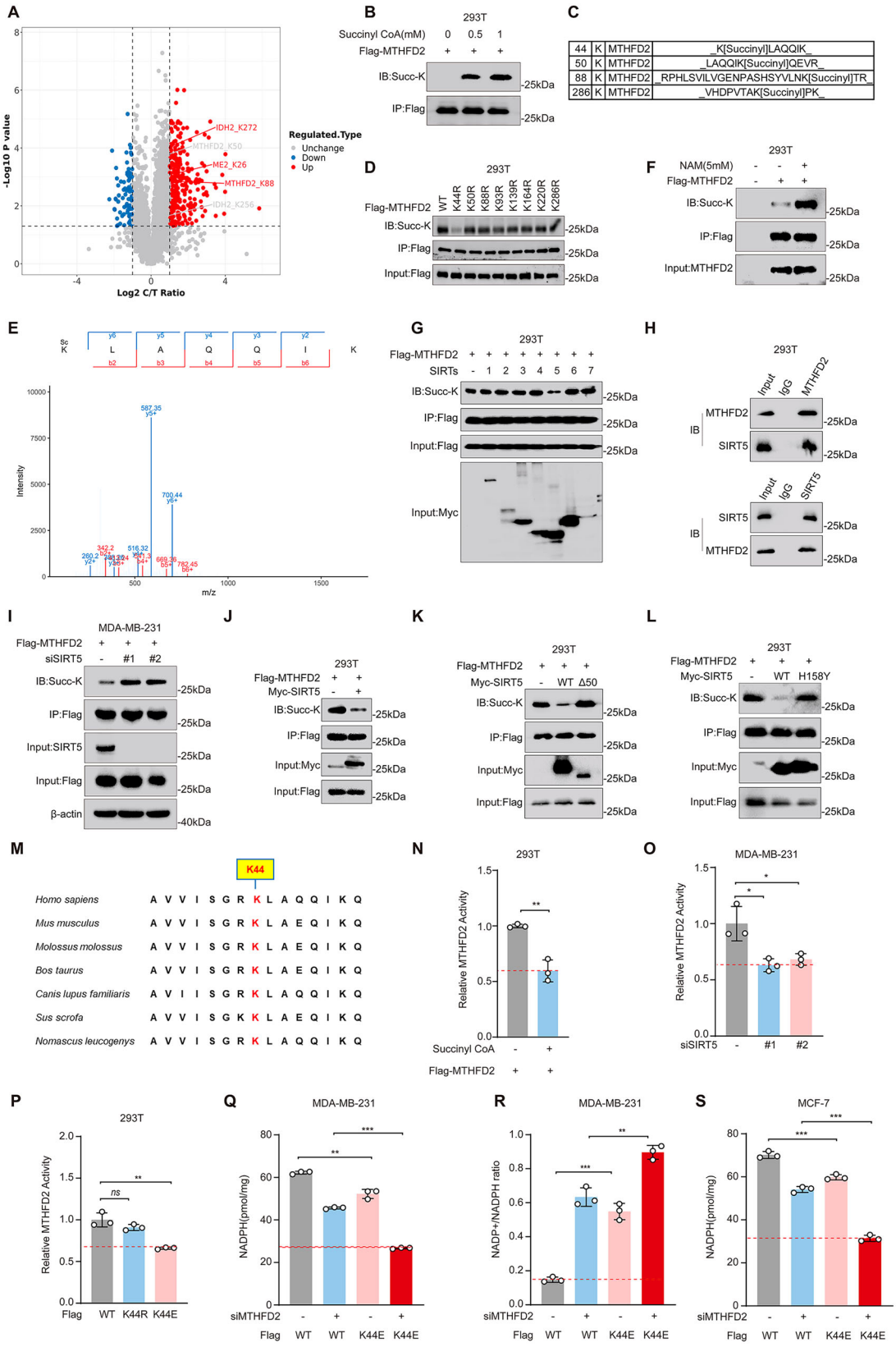

K44 reduces MTHFD2 enzymatic activity, while SIRT5-mediated desuccinylation restores MTHFD2 activity. Notably, MTHFD2 is a crucial enzyme that catalyzes the conversion of methylenetetrahydrofolate to tetrahydrofolate using $NADP^+$ as the hydrogen acceptor, generating NADPH during one-carbon metabolism[47]. Since SIRT5-mediated desuccinylation activates MTHFD2 enzymatic activity, we hypothesized that succinylated MTHFD2 might influence the production of the downstream metabolite NADPH. To test this hypothesis, we overexpressed FLAG-tagged WT MTHFD2 or the MTHFD2 mutant (K44E) in MDA-MB-231 cells with or without MTHFD2 knockdown and measured NADPH production. We

Fig. 2 | SIRT5 activates MTHFD2 activity through desuccinylation and promotes NADPH production. A Volcano plot of changes in MTHFD2, ME2, and IDH2 succinylation modification sites in U2OS cells treated with 20 μM Etoposide. **B** In vitro MTHFD2 succinylation assay. MTHFD2 proteins were incubated with different concentrations of succinyl-CoA. Protein succinylation levels were analyzed by western blotting. **C** Possible succinylation sites of MTHFD2 identified by LC-MS. **D** Measurement of MTHFD2 succinylation in HEK293T cells transfected with Flag-tagged wide-type (WT) or mutant (K44R, K50R, K88R, K93R, K139R, K164R, K220R, and K286R) MTHFD2. MTHFD2-Flag was immunoprecipitated and its succinylation was examined with a pan-succinylated lysine antibody. **E** Identification of succinylated peptides around MTHFD2 K44 as determined by mass spectrometry. **F** Succinylation levels of ectopically expressed MTHFD2 in HEK293T cells were measured. Cells were treated with 5 mM NAM for 3 h before harvesting. MTHFD2-Flag was immunoprecipitated from cell lysates and its succinylation was examined with a pan-succinylated lysine antibody. **G** SIRT5, instead of other sirtuins, decreases MTHFD2 succinylation level. HEK293T cells were cotransfected with Flag-tagged MTHFD2 and Myc-tagged SIRT1, SIRT2, SIRT3, SIRT4, SIRT5 or SIRT6. Precipitated SHMT2 proteins or ectopically expressed SIRT3, SIRT4, or SIRT5 were determined. Relative succinylation level was quantified. **H** Endogenous interaction of SIRT5 and MTHFD2 in HEK293T cells. **I** The effect of knockdown of SIRT5 on succinylation of MTHFD2 in MDA-MB-231 cells. **J** SIRT5 decreases the MTHFD2 succinylation level. Myc-SIRT5 plasmid was transfected into HEK293T cells. The MTHFD2 succinylation level was detected by western blotting. **K** SIRT5 mainly desuccinylates MTHFD2 in mitochondria. Flag-tagged MTHFD2 and Flag-tagged SIRT5 or mitochondrial transit peptide defective SIRT5Δ50 were cotransfected into HEK293T cells. Succinylation of precipitated MTHFD2 was determined. Relative succinylation level was quantified. **L** WT SIRT5 but not its catalytic-dead H158Y mutant decreases the MTHFD2 succinylation level. WT SIRT4 and H158Y mutants were transfected into HEK293T cells. The MTHFD2 succinylation level was detected by western blotting. **M** The K44 residue of MTHFD2(marked red) is evolutionarily conserved. **N** In vitro succinylation of MTHFD2 decreased its activity. MTHFD2 proteins were purified and incubated with or without 100 μM succinyl-CoA for 30 min at 37 °C before western blotting and MTHFD2 enzymatic assays were performed. Unpaired two-tailed t-test was used for statistical analyses. **O** MTHFD2 enzyme activity was determined after SIRT5 knockdown. MTHFD2 enzymatic activity was quantified. **P** K44E mutation decreased MTHFD2 activity. Different MTHFD2 plasmids were transfected into HEK293T cells, and MTHFD2 proteins were purified from these cells and subjected to MTHFD2 enzymatic activity analyses. **Q** NADPH levels in MDA-MB-231 cells overexpressing Different MTHFD2 plasmids in the absence of MTHFD2 siRNA are shown. **R** $NADP^+$/NADPH ratio in MDA-MB-231 cells overexpressing Different MTHFD2 plasmids in the absence of MTHFD2 are shown. **S** NADPH levels in MCF-7 cells overexpressing Different MTHFD2 plasmids in the absence of MTHFD2 siRNA are shown.

found that only overexpression of WT MTHFD2 was able to rescue the decrease in NADPH levels caused by MTHFD2 depletion in MDA-MB-231 cells. In contrast, overexpression of the MTHFD2 mutant (K44E) not only failed to rescue the NADPH decrease(Fig. 2Q) but also significantly increased the $NADP^+$/NADPH ratio in MTHFD2-depleted cells (Fig. 2R). Similarly, in breast cancer MCF-7 cells with MTHFD2 knockout, only overexpression of wild-type MTHFD2 was able to rescue the reduction in NADPH levels caused by MTHFD2 loss (Fig. 2S). These findings suggest that succinylation of MTHFD2 at lysine K44 affects NADPH levels by reducing MTHFD2 enzymatic activity.

Depletion of MTHFD2 enhances ROS levels and induces cellular senescence

While our findings demonstrate that SIRT5 enhances MTHFD2 enzymatic activity via desuccinylation, thereby promoting NADPH production, the extent to which MTHFD2 itself contributes to the regulation of cellular senescence remains unclear. To investigate this, we constructed models of OIS, replicative senescence (RS), chemotherapeutic drug (ETOP)-induced senescence model (CIS), and hydrogen peroxide (H_2O_2)-induced senescence using early-passage human foreskin fibroblast HFF cells (P18), and assessed MTHFD2 expression in both young and senescent cells. We found that the mRNA levels and protein levels of MTHFD2 were reduced in OIS models (Fig. 3A, B). In our replicative senescence model, we used HFF cells subjected to continuous passaging to induce cellular aging. Cells were passaged approximately every 3–4 days at a 1:3 split ratio, and the passage number (P) was recorded to track cumulative divisions. We observed that as HFFs progressed from early passages (e.g., P10) to late passages (e.g., P50), there was a gradual increase in the senescence marker p21, accompanied by a progressive decline in MTHFD2 protein levels (Fig. 3C). Similarly, MTHFD2 protein levels progressively declined with increasing cellular senescence in both the CIS model induced by 50 μM ETOP for 48 hours and the senescence model induced by 100 μM H_2O_2 for 1 h (Supplementary Fig. 3A, Fig. 3D). These findings suggest a selective loss of MTHFD2 protein during cellular senescence. To investigate the underlying mechanisms responsible for this decline, we first examined whether MTHFD2 downregulation occurs at the transcriptional level. RT–qPCR analysis revealed that although MTHFD2 mRNA levels were moderately reduced in OIS and CIS models, the extent of reduction was notably less than that observed at the protein level (Fig. 3B, Supplementary Fig. 3A). Notably, MTHFD2 mRNA levels remained largely unchanged in RS of human foreskin fibroblasts (HFFs) and in H_2O_2-induced senescence (Supplementary Fig. 3B, C), suggesting that the decline in MTHFD2 protein during senescence is unlikely to be driven by transcriptional downregulation in these contexts. To further delineate the mechanism responsible for MTHFD2 protein loss during senescence, we treated cells with the proteasome inhibitor MG132 (0.5 μM), which failed to restore MTHFD2 protein levels in senescent cells (Supplementary Fig. 3D, E), suggesting that proteasome-mediated degradation was not involved. By contrast, treatment with the lysosome inhibitor Lys05—a dimeric analogue of chloroquine[48] that blocks autophagosome-lysosome fusion—markedly restored MTHFD2 protein levels in both IMR90 cells (OIS) and HFF cells (RS) (Fig. 3E, Supplementary Fig. 3F). Furthermore, silencing of the upstream autophagy regulator ATG5 impaired the downregulation of MTHFD2 in senescent IMR90 cells (Fig. 3F), further implicating the autophagy–lysosome pathway in mediating MTHFD2 degradation. To investigate whether MTHFD2 serves as an autophagic substrate during cellular senescence, we performed immunofluorescence staining for endogenous MTHFD2. In senescent cells, we observed an increased number of cytoplasmic MTHFD2 puncta that colocalized with LC3 (Fig. 3G), a key autophagy-related protein responsible for substrate recognition and delivery to autophagosomes[49]. Similarly, enhanced colocalization of endogenous MTHFD2 with the lysosomal marker LAMP1[50] was also evident in senescent cells (Fig. 3H). These findings further support that MTHFD2 undergoes cytoplasmic autophagy–lysosome–mediated degradation during senescence, and suggest that this mechanism may play a central role in the downregulation of MTHFD2 protein levels in senescence cells.

It is well known that ROS play a crucial role in cell differentiation and homeostasis[51]. ROS and oxidative stress can lead to mitochondrial dysfunction and exacerbate cell senescence[52–55]. Notably, NADPH is a crucial intracellular antioxidant that helps regulate ROS homeostasis. Therefore, we wanted to explore whether MTHFD2-mediated ROS homeostasis has a regulatory role in cell senescence. We first investigated the impact of MTHFD2 depletion on the induction of cellular senescence. Unexpectedly, in normal diploid fibroblast IMR90 cells, a well-established senescence model, silencing MTHFD2 with siRNA resulted in G0/G1 arrest (Fig. 3I). This implies that depletion of MTHFD2 may lead to cell growth arrest. To further investigate the impact of MTHFD2 depletion on cellular senescence, young HFF cells (P18) were subjected to MTHFD2 knockdown, and cell senescence was subsequently examined. We found that MTHFD2 knockdown led to increased senescence-associated β-galactosidase (SA-β-gal) staining in young HFF cells (P18) (Fig. 3J). Importantly, we observed that overexpression of MTHFD2 in senescent HFF cells (P40) showed a reduced percentage of SA-β-gal positive cells compared to control cells (Fig. 3K). These data suggest that

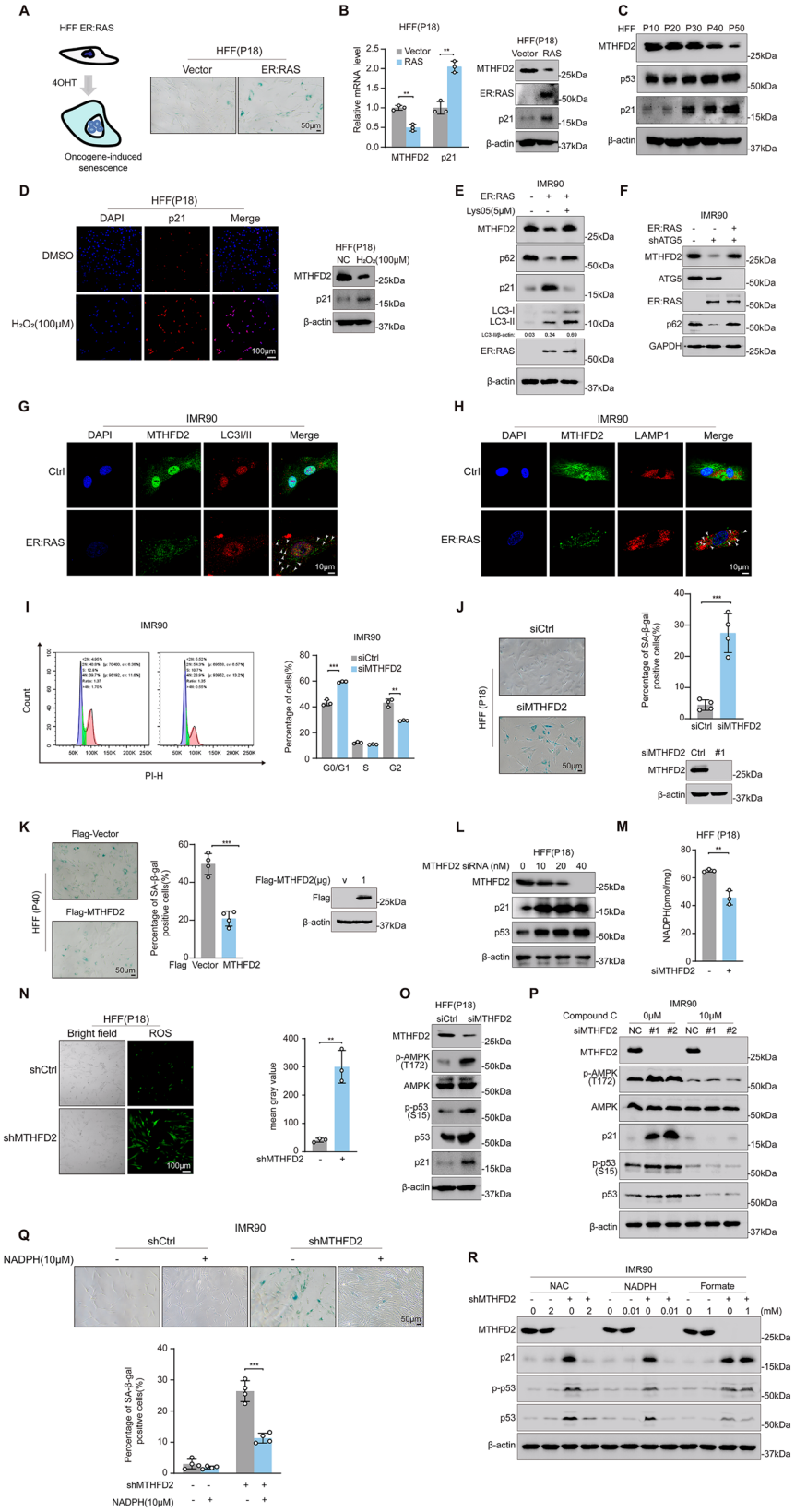

Fig. 3 | Depletion of MTHFD2 enhances ROS levels and induces cellular senescence. A RAS-induced senescence (OIS) in HFF cells (P18). Left: oncogene RAS-induced cell senescence schematic. Right: SA-β-gal staining in oncogene RAS-induced cell senescence. **B** qPCR (Left) and Immunoblots (Right) of MTHFD2 and p21 in oncogene RAS-induced cell senescence. **C** Immunoblots of MTHFD2 and p21 in replicative cell senescence models. **D** Immunofluorescence of p21 (Left), and immunoblot of MTHFD2 and p21 (Right) in H_2O_2-induced senescence model. HFF (P18) were treated with 100 μM H_2O_2 for 1 h. **E** Expression of the indicated proteins was determined by immunoblot in IMR90 cells transfected with vehicle control or ER: RAS to induce senescence with or without simultaneous treatment of Lys05 (5 μM). **F** Expression of the indicated proteins was determined by immunoblot in IMR90 cells with or without ATG5 knockdown. **G**, **H** Immunofluorescence of MTHFD2 co-localization with specific for autophage (LC3I/II) and lysosomal marker LAMP1. **I** IMR90 cells were transfected with control or MTHFD2 siRNAs, the cell cycle progression was detected by flow cytometry analysis. **J** Effect of MTHFD2 silencing (siMTHFD2) and siControl on cellular senescence. HFF (P18) were cultured in medium and then transfected with siMTHFD2 and siControl, respectively. The cellular senescence was indicated by SA-β-gal staining. **K** Effect of MTHFD2 overexpression (3xFlag-MTHFD2) and vector on cellular senescence. HFF (P40) were cultured in medium and then transfected with 3xFlag-MTHFD2 and 3xFlag-Vector, respectively. The cellular senescence was indicated by SA-β-gal staining. **L** Protein expression in HFF cells (P18) treated with control siRNA (−) or increasing amounts of MTHFD2 siRNA for 48 h was analyzed by Western blot using the indicated antibodies. Data are representative of three independent experiments. **M** HFF cells (P18) were transfected with control or MTHFD2 siRNAs, the NADPH levels was detected. **N** HFF cells (P18) transfected with MTHFD2 siRNA or control siRNA, the relative ROS level was determined by immunofluorescence. **O** Protein expression in HFF cells (P18) treated with control siRNA (−) or MTHFD2 siRNA for 48 h was analyzed by Western blot using the indicated antibodies. Data are representative of three independent experiments. **P** The activation status of p53 and AMPK was evaluated in IMR90 cells transfected with either control siRNA or MTHFD2-targeting siRNA, in the presence or absence of the AMPK inhibitor Compound C (10 μM). **Q** Cellular senescence was assessed by SA-β-gal staining in IMR90 cells with or without MTHFD2 silencing, in the presence or absence of exogenous NADPH (10 μM). **R** The protein expression levels of p53 and its downstream target p21 were examined in IMR90 cells treated with or without NAC (2 mM), NADPH (10 μM), or Formate (1 mM), in the presence or absence of MTHFD2 knockdown.

MTHFD2 depletion may contribute to replicative cellular senescence, while overexpression of MTHFD2 can alleviate it.

To further investigate the molecular mechanism of MTHFD2 depletion-induced cellular senescence, we examined the expression of the senescence-related marker p21 following MTHFD2 knockdown using different concentrations of siRNA in HFF cells. We found that MTHFD2 knockdown not only increased p21 protein levels but also activated p53 expression (Fig. 3L). It is well known that p53 is essential for the induction and maintenance of replicative senescence in human cells[56,57]. Thus, these results suggest that MTHFD2 depletion may induce cellular senescence by

activating the p53/p21 signaling pathway. Next, we investigated the regulatory mechanism of MTHFD2 on p53. Since the NAD-dependent metabolic enzyme MTHFD2 plays an important role in carbon metabolism and ROS homeostasis[58], we speculated that MTHFD2 depletion might affect NADPH levels and, consequently, ROS levels during cellular senescence. To verify this, we assessed changes in NADPH and ROS levels in MTHFD2-silenced cells. We found that MTHFD2 knockdown significantly reduced NADPH levels and markedly increased intracellular ROS levels in HFF cells (P18) (Fig. 3M, N). This demonstrates that MTHFD2 maintains ROS homeostasis during replicative senescence by regulating NADPH production. ROS is known to activate the classical energy sensor AMP-activated protein kinase (AMPK), which can subsequently phosphorylate and activate p53[59,60]. Thus, we hypothesized that MTHFD2 depletion might induce cellular senescence by increasing ROS levels, which could affect AMPK expression and subsequently mediate the expression of p53 and its target gene CDKN1A (encodes p21). To test this, we analyzed the expression of various proteins following MTHFD2 knockdown in young HFF cells (P18). We found that MTHFD2 knockdown activated AMPK and led to upregulation of p-p53 and its target gene p21 (Fig. 3O). Similarly, we assessed changes in p-AMPK (T172) after MTHFD2 knockdown using a temporal gradient of siRNA. We observed that MTHFD2 knockdown upregulated p-AMPK (T172) in a time-dependent manner and significantly increased p53 and p21 levels (Supplementary Fig. 3G). This suggests that MTHFD2 depletion induces cellular senescence by activating p-AMPK, which then further activates p-p53 and its target gene p21. We investigated whether AMPK is necessary for MTHFD2-induced p53 activation by knocking it down in mouse embryonic fibroblasts (MEF) cells and comparing AMPK-null and wild-type MEFs. As we observed, in the case of AMPK overexpression, depletion of MTHFD2 significantly increased the expression levels of p-AMPK and p53. In contrast, when AMPK was knocked down or knocked out, MTHFD2 depletion significantly reduced the ability to activate p-p53 and p21 expression (Supplementary Fig. 3H). These findings indicate that AMPK serves as a critical upstream regulator of the p53–p21 axis in response to MTHFD2 depletion. To further assess whether MTHFD2 depletion activates the AMPK–p53–p21 axis, we treated IMR90 cells with 10 μM Compound C, a selective AMPK inhibitor, and examined the expression of p53 and p21. Inhibition of AMPK markedly attenuated MTHFD2 depletion-induced phosphorylation of p53 and significantly reduced p21 expression (Fig. 3P), supporting the involvement of AMPK signaling in this pathway. Notably, in human cells, MTHFD2-mediated one-carbon metabolism not only contributes to NADPH production but also facilitates the generation of folate intermediates such as N^5, N^{10}-methenyl-THF and N^{10}-formyl-THF. Moreover, formate produced via this metabolic pathway is further converted into N^{10}-formyl-THF and N^5, N^{10}-methenyl-THF (Supplementary Fig. 3I). To further assess the functional involvement of MTHFD2-derived NADPH in the regulation of cellular senescence, we employed the X-tremeGENE HP DNA transfection reagent to facilitate direct intracellular delivery of NADPH in IMR90 cells. This approach led to a marked elevation in intracellular NADPH levels, confirming the effectiveness of this delivery strategy (Supplementary Fig. 3J). We found that supplementation with NADPH (10 μM) significantly attenuated the increase in SA-β-gal activity induced by MTHFD2 knockdown in IMR90 cells (Fig. 3Q). Similarly, treatment with N-acetylcysteine (NAC, 2 mM), a ROS scavenger, partially reduced the elevated SA-β-gal activity associated with MTHFD2 depletion (Supplementary Fig. 3K). In contrast, supplementation with formate (1 mM), a one-carbon metabolism intermediate, failed to rescue the senescence phenotype (Supplementary Fig. 3L). These results suggest that the reduction in NADPH levels resulting from MTHFD2 depletion is the principal driver of cellular senescence in this context. Similarly, to further validate that elevated ROS levels resulting from decreased NADPH are responsible for p53/p21 axis activation and subsequent senescence, we examined the expression of p53 and its downstream target p21 in IMR90 cells following MTHFD2 knockdown, with or without supplementation of NAC, NADPH, or formate. We observed that both NAC and NADPH markedly reduced the elevated levels of phosphorylated p53 and p21 induced by MTHFD2 silencing, whereas formate had no such effect (Fig. 3R). Collectively, these findings indicate that depletion of MTHFD2 leads to a reduction in intracellular NADPH levels, resulting in elevated ROS accumulation and subsequent induction of cellular senescence via activation of the AMPK–p53–p21 signaling axis. Furthermore, MTHFD2-derived NADPH plays a critical role in maintaining redox homeostasis and preventing ROS levels from surpassing the threshold necessary to trigger senescence.

SIRT5 mediates the desuccinylation of MTHFD2 to maintain ROS homeostasis and delay cellular senescence

To investigate the impact of SIRT5-mediated desuccinylation of MTHFD2 on cellular senescence, we first examined the regulatory relationship between SIRT5 and MTHFD2 in fibroblast cell lines HFF and IMR90. Indeed, we detected succinylation of MTHFD2 in both HFF (P10) and IMR90 cells (Supplementary Fig. 4A–B), observed a physical interaction between SIRT5 and MTHFD2 (Supplementary Fig. 4C), and confirmed that SIRT5 is responsible for the desuccinylation of MTHFD2 (Supplementary Fig. 4D–F). These findings further support the notion that SIRT5-mediated regulation of MTHFD2 desuccinylation is a conserved mechanism, which may play a critical role in modulating cellular senescence. Since succinylation occurring at the K44 site decreases the enzymatic activity of MTHFD2, we speculated that high succinylation of MTHFD2, leading to changes in its activity, might affect cellular senescence by mediating ROS homeostasis. To test this hypothesis, we generated an MTHFD2 K44E mutant to mimic the negatively charged state of succinylated lysine. FLAG-tagged wild-type MTHFD2 and the K44E mutant were ectopically expressed in replicative senescent HFF cells (P30) with MTHFD2 knockdown to evaluate their capacity to restore intracellular ROS homeostasis. After overexpressing Flag-tagged WT MTHFD2 or MTHFD2 mutant (K44E) in HFF cells (P30) with MTHFD2 knockdown, we observed that only WT MTHFD2 overexpression reduced the high ROS levels resulting from MTHFD2 knockdown, whereas MTHFD2 mutant (K44E) exacerbated ROS levels (Fig. 4A). This suggests that succinylation of MTHFD2 at the K44 site strongly elevates intracellular ROS levels. Next, we further explore the effect of MTHFD2 succinylation at the K44 site on replicative cellular senescence. We overexpressed either wild-type MTHFD2 or the K44E mutant in replicative HFF cells (P30) with or without MTHFD2 knockdown and assessed SA-β-gal activity to evaluate the ability of MTHFD2 succinylation at K44 to rescue MTHFD2 knockdown-induced cellular senescence. As we observed previously, MTHFD2 knockdown significantly increased the number of SA-β-gal-positive HFF cells, whereas overexpression of WT MTHFD2 alleviated cellular senescence (Fig. 4B). Notably, compared to WT MTHFD2, overexpression of the MTHFD2 mutant (K44E) not only failed to rescue SA-β-gal-positive HFF cells but also exacerbated the extent of staining (Fig. 4B). These findings suggest that succinylation of MTHFD2 at the K44 site influences cellular senescence. Interestingly, we observed that adding the ROS scavenger NAC (2 mM) significantly reduced the number of SA-β-gal positive cells caused by MTHFD2 knockdown and overexpression of MTHFD2-K44E in HFF cells (Fig. 4C). These data further suggest that succinylation of MTHFD2 at the K44 site induces cellular senescence by reducing MTHFD2 activity and increasing intracellular ROS levels. Given the selective loss of MTHFD2 in replicative HFF cells at late passage (P50) (Fig. 3C), we next aimed to investigate the causal relationship between MTHFD2 depletion–induced ROS accumulation and the progression of cellular senescence. To evaluate the functional consequences of elevated ROS in MTHFD2-deficient cells, we assessed SA-β-gal activity in late-passage HFF cells (P50) treated with or without the ROS scavenger NAC (2 mM). NAC treatment partially attenuated SA-β-gal activity in these cells (Fig. 4D). Similarly, targeted NADPH supplementation via transfection using X-tremeGENE HP DNA Transfection Reagent also led to a reduction in SA-β-gal activity in late-passage HFF cells (P50) (Supplementary Fig. 4G, H). These findings further suggest that reduced NADPH availability or disrupted redox homeostasis represents a critical driver of cellular senescence upon MTHFD2 depletion. It is well known that SIRT activity is crucial

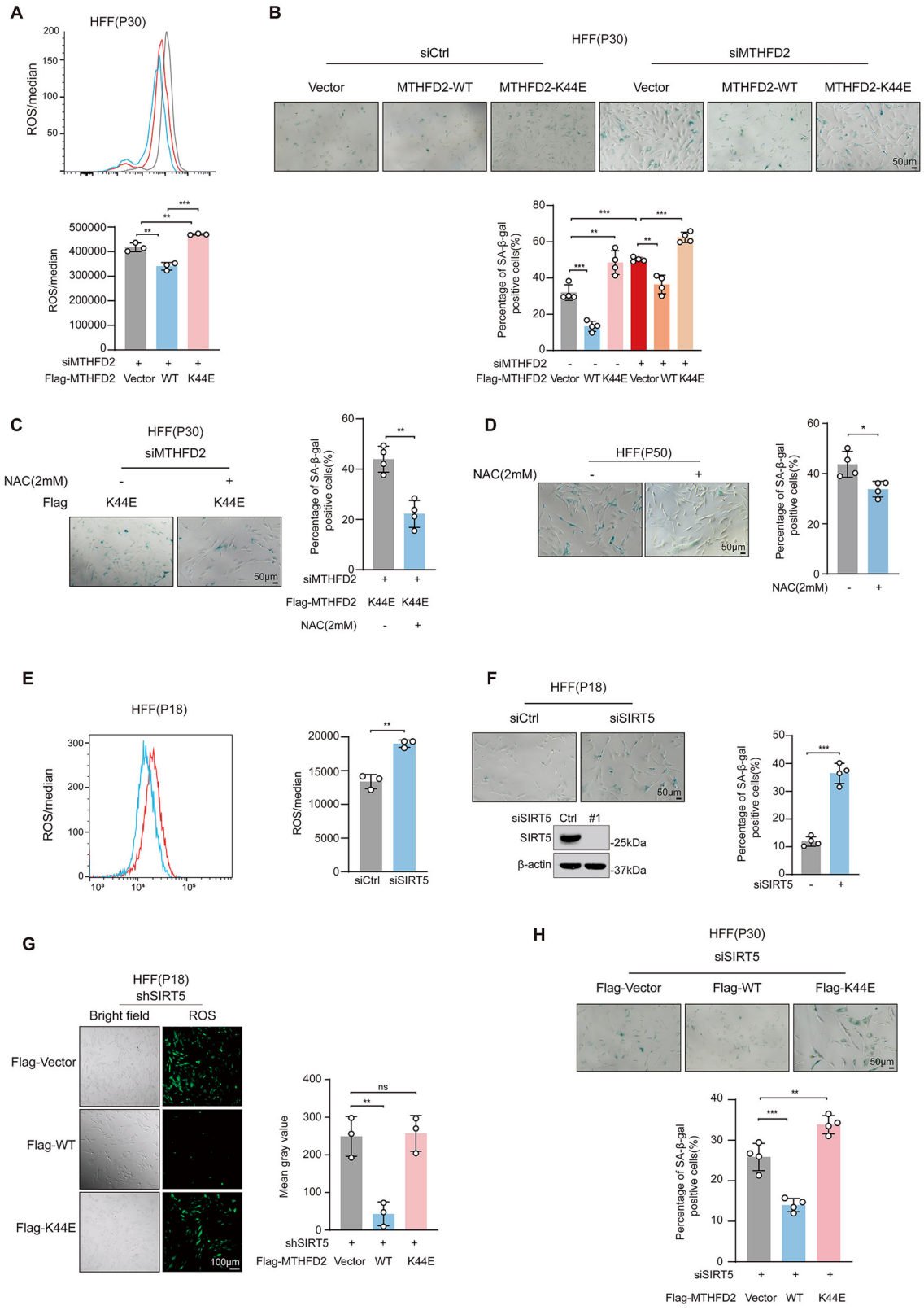

in cellular senescence-related pathways and is closely linked to lifespan[61,62]. Recent studies have shown that deletion of any SIRT1-7 members in MSCs accelerates cellular senescence[63]. Since SIRT5-mediated desuccinylation of MTHFD2 influences NADPH production by activating MTHFD2, SIRT5 might impact cellular senescence by affecting ROS homeostasis. Indeed, we found that SIRT5 knockdown significantly increased intracellular ROS levels (Fig. 4E), and strongly induced cellular senescence (Fig. 4F). Similarly, after overexpressing Flag-tagged WT MTHFD2 or MTHFD2 mutant (K44E) in replicative senescent HFF cells (P30) with SIRT5 knockdown, we found that only WT MTHFD2 overexpression reduced the high ROS levels caused by SIRT5 knockdown, while MTHFD2 mutant (K44E) not only failed to reduce ROS levels but also further increased them in SIRT5-

Fig. 4 | SIRT5 mediates the desuccinylation of MTHFD2 to maintain ROS homeostasis and delay cellular senescence. A HFF cells (P30) that express FLAG-MTHFD2 and FLAG-MTHFD2 K44E were transfected with siMTHFD2, the ROS level was determined by flow cytometry analysis. **B** Effect of ectopic expression of WT MTHFD2 and MTHFD2 K44E mutant on cellular senescence. HFF cells (P30) were transfected with siMTHFD2 or siControl to knock down the endogenous MTHFD2, and then express FLAG-MTHFD2 and FLAG-MTHFD2 K44E. The cellular senescence was indicated by SA-β-gal staining. **C** HFF cells (P30) that were transfected with siMTHFD2 to knock down the endogenous MTHFD2, and express FLAG-MTHFD2 K44E, and add or not add the 2 mM ROS scavenger(NAC), the ROS level was determined by immunofluorescence. **D** Senescence-associated β-galactosidase activity was assessed in serially passaged HFF cells (P50) following treatment with NAC (2 mM). **E** HFF cells (P18) transfected with SIRT5 siRNA or control siRNA, the relative ROS level was determined by flow cytometry analysis. **F** Effect of SIRT5 silencing (siSIRT5) and siControl on HFF (P18) cellular senescence. **G** HFF (P18) were cultured in medium and then transfected with siSIRT5 and siControl, respectively. The cellular senescence was indicated by SA-β-gal staining. **H** HFF cells (P30) were transfected with siRNA to knock down the endogenous SIRT5, and then expressed FLAG-MTHFD2 and FLAG-MTHFD2 K44E. The cellular senescence was indicated by SA-β-gal staining.

silenced cells (Fig. 4G). Similarly, overexpression of MTHFD2-K44E did not reduce the number of SA-β-gal positive cells caused by SIRT5 knockdown, whereas WT-MTHFD2 did (Fig. 4H). Taken together, these results suggest that both MTHFD2 depletion and hyper-succinylation can induce cellular senescence, whereas SIRT5-mediated desuccinylation of MTHFD2, acting as a 'longevity factor,' activates MTHFD2 enzymatic activity to maintain normal intracellular ROS homeostasis and slow down cell senescence.

Depletion of MTHFD2 decreases breast cancer cell proliferation and chemotherapy drug resistance

Alterations in folate metabolism or increased expression of one-carbon metabolic enzymes have been linked to higher cancer risk[49]. An analysis of public gene-expression databases (http://www.oncomine.org) showed that MTHFD2 expression was significantly upregulated in breast cancers. Additionally, high MTHFD2 expression was significantly associated with poor prognosis in breast cancers (Fig. 5A, B). This suggests that MTHFD2 may be a potential oncogene. To further investigate, we used the CCK8 assay to assess the proliferation ability of breast cancer MDA-MB-231 with MTHFD2 knockdown. The results indicated that MTHFD2 knockdown reduced the proliferation rate of MDA-MB-231 tumor cells compared to the control group (Fig. 5C). Similarly, experiments using the thymidine analogue EdU (5-ethynyl-2'-deoxyuridine) during DNA synthesis showed that MTHFD2 overexpression significantly increased DNA synthesis during cell proliferation (Fig. 5D). This suggests that MTHFD2 acts as a carcinogenic factor that promotes tumor proliferation. In order to investigate the molecular mechanism of MTHFD2 in inhibiting tumor cell proliferation. We treated MDA-MB-231 cells with two different DNA damage inducers, olaparib and doxorubicin (DOX). We found that MTHFD2 protein levels increased with higher concentrations of olaparib and DOX (Fig. 5E, F). This suggests that MTHFD2 expression may rise in response to DNA damage caused by chemotherapeutic drugs. To explore the mechanism by which MTHFD2 participates in the DNA damage response, we analyzed DNA damage markers by treating MDA-MB-231 cells with or without MTHFD2 knockdown with ETOP. We found that MTHFD2 knockdown increased the expression levels of DNA damage markers γH2AX and p-RPA2 (Fig. 5G). Immunofluorescence experiments also showed that MTHFD2 knockdown in MCF-7 cells exacerbated γH2AX expression (Fig. 5H). These results suggest that MTHFD2 responds to DNA damage induced by chemotherapeutic drugs, which may contribute to its role as a tumor-promoting factor. Although knockdown of the MTHFD2 protein reduces tumor cell proliferation, these studies did not address the requirement for the enzymatic activity of MTHFD2. Therefore, catalytically dead construct (Gln132Lys/Asp155Ala) carrying point mutations in the tetrahyrofolate (THF)-binding pocket (Gln132Lys/Asp155Ala-MTHFD2) was constructed, and overexpressing Flag-tagged WT MTHFD2 or Gln132Lys/Asp155Ala-MTHFD2 (Q132K/D155A-MTHFD2) in MDA-MB-231 cells with MTHFD2 knockdown. We observed that only WT MTHFD2 overexpression can increase the cell proliferation resulting from MTHFD2 knockdown, but not Q132K/D155A-MTHFD2 (Fig. 5I). Similarly, in MTHFD2 knockdown MDA-MB-231 cells, only WT MTHFD2 overexpression can decreased the expression of the DNA damage marker γ-H2AX resulting from MTHFD2 knockdown, but not Q132K/D155A-MTHFD2 (Fig. 5J). This suggests that the enzyme activity of MTHFD2 is equally important for the regulation of DNA damage repair and the proliferation of tumor cells. MTHFD2 depletion inhibits the proliferation of breast cancer MDA-MB-231 and MCF-7 cells (Fig. 5C, D), which appears to represent a universal mechanism by which MTHFD2 depletion inhibits tumor cell proliferation. However, we note that most chemotherapeutic agents lack efficacy in the treatment of metastatic breast cancer[64]. We speculate that the expression level and metabolic enzyme activity of MTHFD2 may affect the sensitivity of breast cancer cells to chemotherapeutic agents. We treated breast cancer MDA-MB-231 cells with 40 μM olaparib, and examined the cell proliferation, with or without MTHFD2 knockdown. Crystal violet staining confirmed that MTHFD2 knockdown reduced the proliferative capacity of MDA-MB-231 cells and further decreased cell proliferation under olaparib treatment (Fig. 5K). Whereas MTHFD2 overexpression had the opposite effect (Fig. 5L). This suggests that MTHFD2 overexpression increases tumor cell resistance to chemotherapeutic drugs, while MTHFD2 knockdown decreases this resistance. Further, we also examined the effect of the enzymatic activity of MTHFD2 on the chemoresistance of breast cancer cells. EdU experiments revealed that overexpression of WT MTHFD2 enhanced resistance to olaparib in MTHFD2-silenced breast cancer MCF-7 cells (Fig. 5M). These data not only demonstrate that MTHFD2 depletion suppresses the proliferation of breast cancer cells, but also indicate that reduced MTHFD2 expression or enzymatic activity sensitizes these cells to chemotherapeutic agents.

SIRT5 mediates the desuccinylation of MTHFD2 enhances breast cancer cell proliferation and chemoresistance

Lower metabolic enzyme activity of MTHFD2 increases DNA damage and inhibits breast cancer cell proliferation (Fig. 5I, J). Succinylation of MTHFD2 was consistently observed across diverse breast cancer cell lines (Supplementary Fig. 1C–E), with SIRT5 identified as the principal desuccinylase responsible for modulating this post-translational modification (Fig. 2I; Supplementary Fig. 2 Fig. 2B–F). Moreover, endogenous immunofluorescence staining in MDA-MB-231 cells revealed marked co-localization of MTHFD2 and SIRT5 (Fig. 6A), providing further evidence for a SIRT5-dependent regulatory axis governing MTHFD2 desuccinylation in breast cancer. We further explored whether activation of MTHFD2 by SIRT5 is also involved in regulating DNA damage and cell proliferation in breast cancer cells. Not surprisingly, we found that knockdown of SIRT5 in MCF-7 cells increased the expression of the DNA damage marker γ-H2AX (Fig. 6B). Only overexpression of WT MTHFD2 reduced γ-H2AX expression, whereas overexpression of MTHFD2-K44E and Q132K/D155A-MTHFD2 did not (Fig. 6B). This suggests that activation of MTHFD2 activity by SIRT5 can participate in the DNA damage process. Furthermore, we co-transfected MDA-MB-231 cells with either the MTHFD2-K44E mutant or wild-type MTHFD2 (MTHFD2-WT) along with either Myc-SIRT5 (desuccinylase) or Myc-Vector (control), and assessed tumor cell proliferation using EdU staining. We found that SIRT5 overexpression enhanced DNA synthesis during tumor cell proliferation, whereas MTHFD2-K44E overexpression significantly reduced tumor cell proliferation (Fig. 6C). This suggests that SIRT5-mediated desuccinylation of MTHFD2 promotes tumor cell proliferation. Indeed, an analysis of The Cancer Genome Atlas (TCGA) database (https://portal.gdc.com) revealed a positive correlation between SIRT5 and MTHFD2 expression in BRCA (Fig. 6D). This implies that SIRT5's regulation of MTHFD2 is closely associated with breast cancer development. To investigate the role of SIRT5-

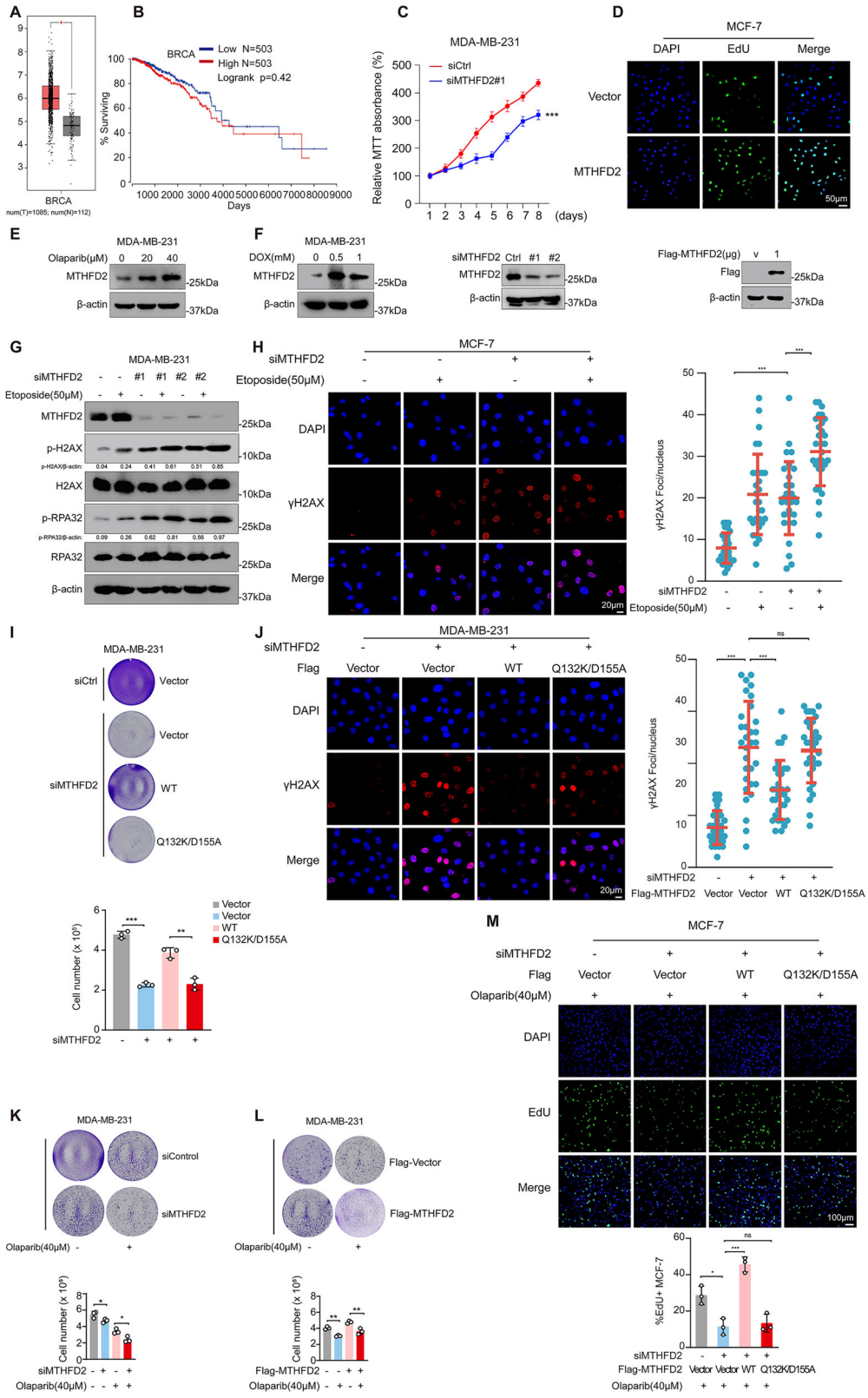

mediated desuccinylation of MTHFD2 in tumor cell chemoresistance, we co-transfected MDA-MB-231 cells with either wild-type MTHFD2 (WT) or the succinylation-deficient mutant MTHFD2-K44E, along with either Myc-SIRT5 or Myc-Vector, and assessed cell proliferation in the presence or absence of olaparib. As expected, olaparib treatment significantly suppressed cell proliferation in control (Vector) groups. However, overexpression of SIRT5 markedly counteracted this inhibitory effect, leading to increased cell proliferation despite olaparib exposure (Fig. 6E), suggesting a role of SIRT5 in promoting chemoresistance. Notably, the MTHFD2-K44E mutant exhibited a significantly reduced capacity to promote cell proliferation compared to WT-MTHFD2 under the same treatment conditions (Fig. 6E). Furthermore, cells co-transfected with SIRT5 and

Fig. 5 | Depletion of MTHFD2 decreases breast cancer cell proliferation and chemotherapy drug resistance. **A** Box plots of MTHFD2 transcript levels in BRCA, the RNA-sequencing expression profiles and corresponding clinical information for multi-cancer were downloaded from the TCGA dataset. The statistical significance computed by the Wilcoxon test is annotated by the number of stars (*p-value < 0.05; **p-value < 0.01; ***p-value < 0.001). **B** Kaplan–Meier survival analysis of the gene signature from TCGA dataset with BRCA based on MTHFD2 expression. **C** MDA-MB-231 cells were transfected with control or MTHFD2 siRNAs, cell proliferation was analyzed by MTT experiment. **D** MCF-7 cells were transfected with 3xFlag-Vector or 3xFlag-MTHFD2, cell proliferation was analyzed by EdU-488 experiment. **E** MDA-MB-231 cells treated with 0, 20 and 40 μM Olaparib for 48 h, and protein expression were analyzed. **F** MDA-MB-231 cells treated with 0, 0.5 and 1 mM Doxorubicin for 48 h, and protein expression were analyzed. **G** MDA-MB-231 cells transfected with control siRNA (−) or MTHFD2 siRNA for 48 h, and treated with 50 μM etoposide for 4 h. Protein expression was analyzed by Western blot using the indicated antibodies. Data are representative of three independent experiments. **H** MCF-7 cells were transfected with control or MTHFD2 siRNAs, γH2AX protein was detected by immunofluorescence. **I** Effect of ectopic expression of WT MTHFD2, MTHFD2 K44E and Gln132Lys/Asp155Ala-MTHFD2 mutant on cell proliferation. MDA-MB-231 cells were transfected with siMTHFD2 or siControl to knock down the endogenous MTHFD2, and then express FLAG-MTHFD2, FLAG-MTHFD2 K44E, and Gln132Lys/Asp155Ala-MTHFD2. The cell proliferation was assayed by crystal violet staining. **J** Effect of ectopic expression of WT MTHFD2, MTHFD2 K44E, and Gln132Lys/Asp155Ala-MTHFD2 mutant on DNA damage. MDA-MB-231 cells were transfected with siMTHFD2 or siControl to knock down the endogenous MTHFD2, and then express FLAG-MTHFD2, FLAG-MTHFD2 K44E and Gln132Lys/Asp155Ala-MTHFD2. The γH2AX protein was detected by immunofluorescence. **K** MDA-MB-231 cells were transfected with control or MTHFD2 siRNAs, and treated with 40 μM Olaparib for 24 h, and cell survival was assayed by crystal violet staining. Protein expression was analyzed by western blot. **L** MDA-MB-231 cells were transfected with Vector or 3xFlag-MTHFD2, and treated with 40 μM Olaparib, and cell survival was assayed by crystal violet staining. **M** Effect of ectopic expression of WT MTHFD2, MTHFD2 K44E, and Gln132Lys/Asp155Ala-MTHFD2 mutant on cell chemoresistance. MCF-7 cells were transfected with siMTHFD2 or siControl to knock down the endogenous MTHFD2 and express FLAG-MTHFD2, FLAG-MTHFD2 K44,E and Gln132Lys/Asp155Ala-MTHFD2, and then treated with 40 μM Olaparib for 48 h. The cell proliferation was assayed by EdU-488.

MTHFD2-K44E proliferated significantly less than those co-transfected with SIRT5 and WT-MTHFD2, even in the presence of olaparib (Fig. 6E). These findings indicate that lysine 44 succinylation of MTHFD2 impairs its ability to support tumor cell resistance to olaparib, highlighting a regulatory role for MTHFD2 succinylation in chemotherapeutic response. To further validate this conclusion, we overexpressed wild-type MTHFD2 (MTHFD2-WT) and the K44E mutant in breast cancer MDA-MB-231 cells, with or without MTHFD2 knockdown, and injected these cells into immunocompromised mice. Tumorigenicity was assessed after intraperitoneal injection of olaparib when tumors reached a volume of 100 mm^3. We observed that olaparib injection reduced tumorigenicity compared to control, and the MTHFD2-K44E mutant further enhanced the inhibitory effect of olaparib on tumor cells (Fig. 6F). This data implies that succinylation of MTHFD2 at K44 decreases tumor cell chemoresistance. Taken together, these results demonstrate that SIRT5-mediated desuccinylation of MTHFD2 enhances tumor cell proliferation and resistance to chemotherapeutic drugs by increasing MTHFD2 enzymatic activity.

SIRT5-mediated desuccinylation of MTHFD2 enhances chemoresistance by reducing breast cancer sensitivity to TIS

Although we have demonstrated that low-level expression of MTHFD2 or impairment of its enzymatic activity may inhibit breast cancer cell proliferation by inducing DNA damage. However, this does not explain the specific mechanism by which high MTHFD2 enhances chemoresistance in tumor cells. Indeed, some chemotherapeutic agents are able to induce DNA damage-associated genotoxic stress and high levels of ROS, prompting cancer cells to enter a similar state of senescence known as TIS. This state is thought to be a proliferative mechanism that can cause cell cycle arrest and suppress tumors. Therefore, we speculate that MTHFD2 depletion may enhance the sensitivity of tumor cells to chemotherapeutic agents by promoting TIS. As we have previously studied, MTHFD2 depletion induces senescence in HFF cells (Fig. 3J). However, it is not clear whether depletion of MTHFD2 enhances TIS in breast cancer cells. To verify this, MDA-MB-231 cells were subjected to shRNA-mediated MTHFD2 knockdown or maintained as controls, followed by treatment with 5 μM olaparib for 7 days. Cellular senescence was subsequently evaluated. We found that MTHFD2 knockdown led to increased SA-β-gal staining in low passage MDA-MB-231 cells (Fig. 7A). Beyond that $p16^{INK4a}$ is considered as a specific biomarker for detecting senescent cells. Immunofluorescence experiments show that knockdown of MTHFD2 increases the expression level of $p16^{INK4a}$ in olaparib-treated MDA-MB-231 cells (Fig. 7B). This suggests that depletion of MTHFD2 enhances TIS in breast cancer cells. Further, we also examined the effect of the enzymatic activity of MTHFD2 on breast cancer cell senescence. Consistently, mutants of Gln132Lys/Asp155Ala-MTHFD2 do not reduce the number of SA-β-gal-positive breast cancer cells resulting from MTHFD2 knockdown. But WT-MTHFD2 can reverse this trend (Fig. 7C). These studies suggest that depletion of MTHFD2 or impaired enzyme activity decreases the chemoresistance of breast cancer cells by enhancing TIS.

Since SIRT5-mediated desuccinylation maintains ROS homeostasis by activating the enzymatic activity of MTHFD2 and reduces senescence in fibroblast HFF cells (Fig. 4F, G). Therefore, we wondered whether SIRT5 regulation of MTHFD2 also affects TIS and enhances chemoresistance in breast cancer cells. To verify this, MDA-MB-231 cells were subjected to shRNA-mediated SIRT5 knockdown or maintained as controls, followed by treatment with 5 μM olaparib for 7 days. Cellular senescence was subsequently evaluated. Interestingly, we observed that knockdown of SIRT5 did induce senescence in breast cancer MDA-MB-231 cells (Fig. 7D), and strongly reduced the proliferation of olaparib-treated breast cancer MDA-MB-231 cells (Fig. 7E). Meanwhile, overexpression of WT-MTHFD2 in MDNA-MD-231 cells significantly reduced the level of SA-β-gal induced by SIRT5 knockdown (Fig. 7F). In contrast, overexpression of MTHFD2-K44E not only failed to reduce the level of SA-β-gal induced by SIRT5 knockdown, but also strongly induced an increase in the expression level of SA-β-gal (Fig. 7F). More importantly, Gln132Lys/Asp155Ala-MTHFD2 also failed to restore TIS caused by SIRT5 knockdown (Fig. 7F). These data suggest that SIRT5-mediated low succinylation of MTHFD2 enhances TIS by activating the enzymatic activity of MTHFD2, which increased chemoresistance in breast cancer cells, but high succinylation of the MTHFD2 in K44 reverses this trend. Notably, the combination of senolytics with pro-senescence has been a novel strategy in tumor therapy[65], and navitoclax has also been shown to be an effective senolytics for breast cancer cells[66]. To further validate whether MTHFD2 is a valid TIS target. MDA-MB-231 breast cancer cells, with or without SIRT5 knockdown and overexpressing either WT-MTHFD2 or MTHFD2-K44E, after a 6-day treatment with 5 μM olaparib, cells were exposed to 2.5 μM navitoclax combined with 5 μM olaparib for 2 days, followed by cell proliferation assessment. We found that co-treatment of navitoclax and olaparib significantly reduced the proliferation of MDA-MB-231 cells with SIRT5 knockdown and overexpressing MTHFD2-K44E (Fig. 7G). To establish xenografts, MDA-MB-231 breast cancer cells were injected into the 4-week-old nude BALB/C mice. When tumor volume reached an average of 60 mm^3, daily treatment with 5 mg/kg olaparib via intraperitoneal (I.P.) was initiated for 3 weeks. After 7 days, navitoclax (25 mg/kg) was added via oral gavage(o.g.) for an additional 2 weeks (Fig. 7H). We observed that olaparib injection reduced tumorigenicity compared to control, and the MTHFD2-K44E mutant further enhanced the inhibitory effect of olaparib on tumor cells. More importantly, co-treatment with navitoclax and olaparib significantly reduced the tumorigenicity of MDA-MB-231 cells with SIRT5 knockdown and overexpressing MTHFD2-K44E (Fig. 7I). These data further suggest that succinylation of MTHFD2 occurring at the K44 site enhances TIS and

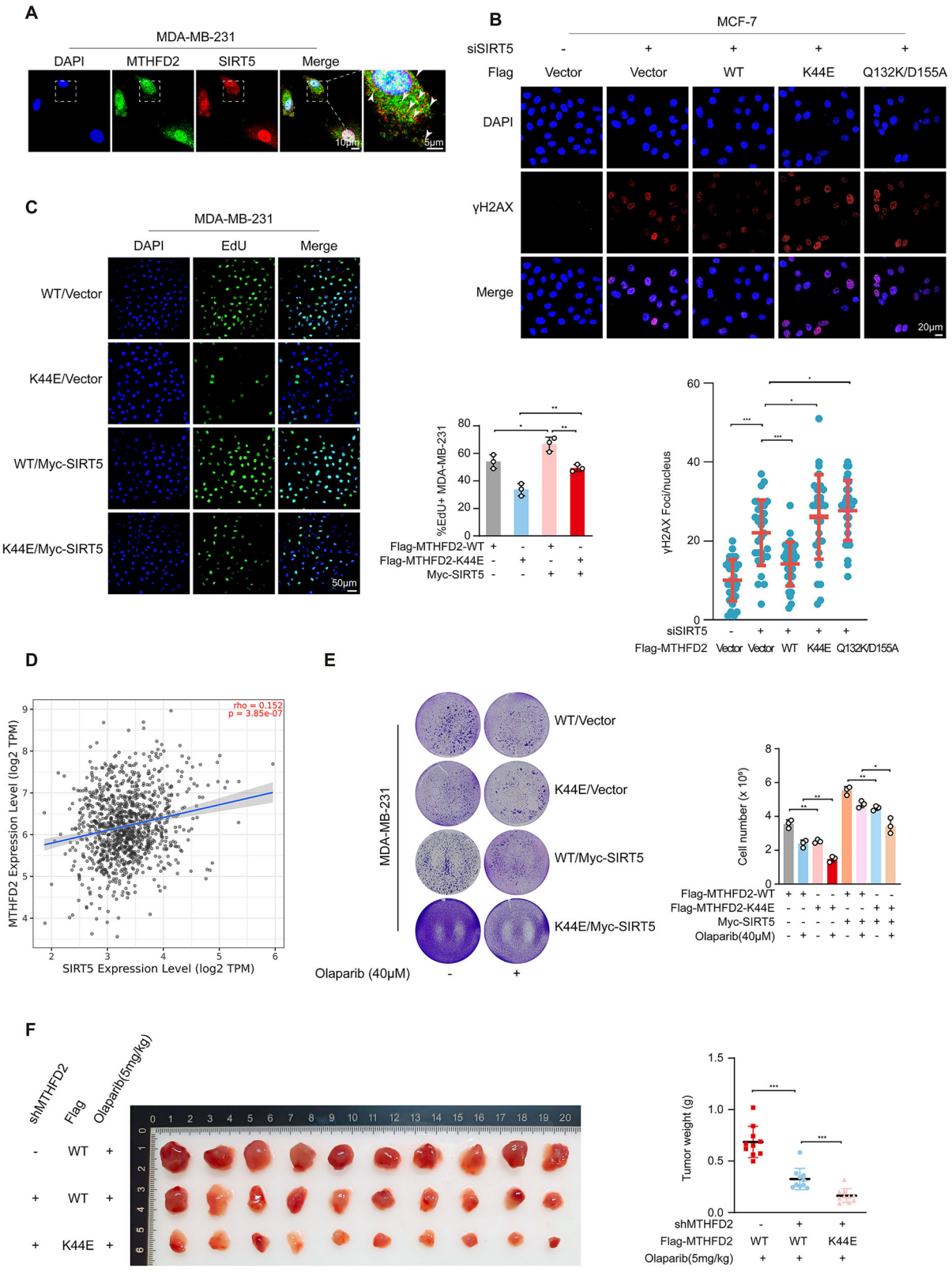

decreases chemoresistance of breast cancer cells. However, this effect is can be blocked by SIRT5.

Discussion

Indeed, abnormalities in post-translational modifications, such as protein lysine succinylation, can contribute to the development of cancer[67]. Chemotherapeutic agents are commonly used in cancer treatment due to their ability to induce DNA damage in cells. However, research has demonstrated that the DNA damage response in tumor cells significantly impacts the efficacy of radiotherapy and chemotherapy[68]. Recent studies have found that some PTMs involved in DNA damage repair proteins, such as lactylation and acetylation modifications, modulate chemoresistance in

Fig. 6 | SIRT5 mediates the desuccinylation of MTHFD2 enhances breast cancer cell proliferation and chemoresistance. A Immunofluorescence of MTHFD2 co-localization with SIRT5. **B** Effect of ectopic expression of WT MTHFD2, MTHFD2 K44E and Gln132Lys/Asp155Ala-MTHFD2 mutant on DNA damage. MCF-7 cells were transfected with siSIRT5 or sicontrol to knock down the endogenous SIRT5, and then express FLAG-MTHFD2, FLAG-MTHFD2 K44E and Gln132Lys/Asp155Ala-MTHFD2. The γH2AX protein expression was detected by immunofluorescence. **C** MDA-MB-231 cells overexpressing Myc-SIRT5 or Myc-vector control in the presence of 3xFlag-MTHFD2-WT or 3xFlag-MTHFD2-K44E, cell proliferation was analyzed by EdU-488 experiment. **D** RNA-sequencing expression (level 3) profiles and corresponding clinical information for BRCA were downloaded from the TCGA dataset (https://portal.gdc.com). The two-gene correlation map is realized by the R software package ggstatsplot. Spearman's correlation analysis to describe the correlation between quantitative variables without a normal distribution. *P*-values less than 0.05 were considered statistically significant ($^*p < 0.05$). **E** MDA-MB-231 cells overexpressing Myc-SIRT5 or Myc-vector control in the presence of 3xFlag-MTHFD2-WT or 3xFlag-MTHFD2-K44E, and treated with 40 μM Olaparib, cell proliferation was assayed by crystal violet staining. **F** Average images (left) and weights (right) of xenograft tumors (4 weeks, means ± S.D., $n = 5$) generated by control or MTHFD2-silenced MDA-MB-231 cells overexpressing 3xFlag-MTHFD2-WT or 3xFlag-MTHFD2-K44E as indicated. One week later, when the tumors reached a volume of 100 mm^3, Olaparib (5 mg/kg) was intraperitoneally injected once a day for 2 weeks. For all graphs, data are presented as mean ± SD, $^*p < 0.05$, $^{**}p < 0.01$, $^{***}p < 0.001$. Statistical analysis was performed with a paired *t* test.

tumor cells[36,69–71]. Although lysine succinylation is an evolutionarily conserved PTM that has been reported to affect the activity, stability, and localization of a wide range of proteins, particularly metabolic enzymes[72,73]. However, there are fewer studies on the involvement of intracellular succinylated proteins in chemotherapeutic resistance. Thus, it is important to investigate whether lysine succinylation of proteins plays a role in the DNA damage response and affects the effectiveness of chemotherapeutic agents against tumor cells.

In this study, we employed liquid chromatography-mass spectrometry tandem techniques and bioinformatics to analyze proteomic changes following ETOP-induced cellular DNA damage and to quantify the dynamics of protein succinylation in response to this stress. Given that many succinylated proteins are enriched in mitochondria—organelles central to both metabolic homeostasis and redox balance—it is plausible that mitochondrial succinylation may influence cellular responses to chemotherapy. Remarkably, some of these dynamically altered succinylated proteins identified are located in mitochondria and are involved in cellular metabolic processes. Mitochondria are essential for energy metabolism, apoptosis regulation, and cell signaling[74]. Once mitochondrial dysfunction occurs, it leads to dysfunctional ROS and further induces cellular senescence and tumorigenesis[55,75,76]. Succinate and NADPH produced by mitochondrial metabolism can be used as a substrate for succinylation modification and an antioxidant reducing substance, respectively. Therefore, it is likely that tumor cells modulate enzymes responsible for NADPH metabolism in mitochondria through succinylation modifications to enhance their antioxidant defenses and maintain their ability to proliferate rapidly. Here, we found that the enzyme responsible for NADPH metabolism in mitochondria (MTHFD2) undergoes succinylation modification, which inhibits the enzymatic activity of MTHFD2 and reduce intracellular NADPH production. This implies that succinylation modification of metabolic enzymes may be one of the important reasons driving metabolic reprogramming in tumor cells.

As mentioned earlier, ROS dysregulation induces cellular senescence, and NADPH is an important reducing substance to maintain ROS homeostasis[18]. Here, we found that MTHFD2 depletion leads to elevated intracellular ROS levels, which activate AMPK and the p53/p21 axis, inducing cellular senescence. These findings suggest that inducing earlier entry into the senescence program through MTHFD2 depletion may lead to cell cycle arrest and suppression of tumorigenesis. Notably, MTHFD2 depletion in senescent cells resulted from its degradation via the autophagy–lysosome pathway (Fig. 3E–H). While autophagy is broadly recognized as a quality control mechanism that attenuates age-associated decline and supports healthspan and longevity[77], our findings indicate that the selective degradation of specific substrates, such as MTHFD2, may paradoxically exacerbate cellular senescence. This degradation disrupts cellular metabolic balance and ROS homeostasis, thereby accelerating the senescence process. Previous studies have underscored the pivotal roles of the sirtuin family, particularly SIRT5, in the regulation of stem cell aging and inflammation[18,63]. These findings suggest that SIRT5 may be downregulated in senescent cells, potentially impairing its desuccinylation activity. Consistent with this notion, we observed a significant increase in the succinylation level of MTHFD2 in senescent cells (Response Fig. 1A, B), which contrasts with the observed decrease in its protein expression (Fig. 3B, C). Given that lysine succinylation has been shown to modulate protein stability and function[78], we further employed DMK to artificially enhance MTHFD2 succinylation (Supplementary Fig. 2A) and unexpectedly detected a change in its protein stability (Response Fig. 1C). Based on these findings, we hypothesize that reduced SIRT5 activity during senescence leads to elevated succinylation of MTHFD2. This post-translational modification may destabilize MTHFD2 and promote its degradation via the autophagy–lysosome pathway, thereby maintaining its persistently low expression. Such a mechanism could not only contribute to the functional loss of MTHFD2 but may also play a critical role in reinforcing the irreversibility of cellular senescence.

In fact, cellular senescence causes a stable growth arrest of premalignant cells, facilitated by cell cycle protein-dependent kinase inhibitors like $p16^{INK4a}$ and p21, which act as a natural barrier to tumorigenesis[70]. Previous studies have shown that upregulation of MTHFD2 expression in a variety of tumors is thought to be associated with high cancer risk and low prognosis[35]. Similarly, we found that overexpression of MTHFD2 promotes breast cancer cell proliferation, whereas depletion of MTHFD2 reverses this effect. Interestingly, MTHFD2 expression significantly decreases with increasing cellular senescence (Fig. 3A–C), in contrast to its high expression levels observed in breast cancer (Fig. 5A, B). This suggests that inducing cells to enter a senescent state by regulating the expression of MTHFD2 seems to be an effective way to inhibit the proliferation of breast cancer cells. In cancer treatment, most chemotherapeutic agents inhibit tumor cell proliferation by inducing DNA damage and high levels of ROS to promote tumor cells into a similar state of senescence (TIS)[5]. However, most chemotherapeutic agents lack efficacy in the treatment of metastatic breast cancer due to chemoresistance. Therefore, finding metabolic targets that enhance TIS in breast cancer cells and reduce resistance to chemotherapeutic agents may be a critical step in breast cancer treatment. In this study, we identified lysine K44 as a key succinylation site on MTHFD2, which impairs the enzymatic activity of MTHFD2 and strongly induces senescence and sensitivity to chemotherapeutic agents in breast cancer cells. This implies that MTHFD2 is a potent metabolic target for TIS in breast cancer. SIRTs are class III nicotinamide adenine dinucleotide (NAD)-dependent histone deacetylases found in various organisms, playing roles in genome stability, metabolic regulation, and stem cell modulation[79]. Among them, SIRT5 is the only known mitochondrial desuccinylase linked to metabolic disorders and cancer[80,81]. SIRT5-mediated desuccinylation of several metabolic enzymes promotes cancer progression[43,82]. In this study, we observed that higher SIRT5 protein levels are associated with decreased MTHFD2 succinylation. SIRT5 enhances MTHFD2's enzymatic activity and promotes NADPH production by catalyzing MTHFD2 desuccinylation, thereby increasing breast cancer cell resistance to chemotherapeutic agents. As we observed, SIRT5-mediated desuccinylation of MTHFD2 retarded cellular senescence (Fig. 4H), whereas high levels of SIRT5 and MTHFD2 expression greatly accelerated breast cancer cell proliferation (Fig. 6C, E). This further suggests that activation of MTHFD2 activity by SIRT5 via desuccinylation would mediate breast cancer cell proliferation and chemoresistance by affecting

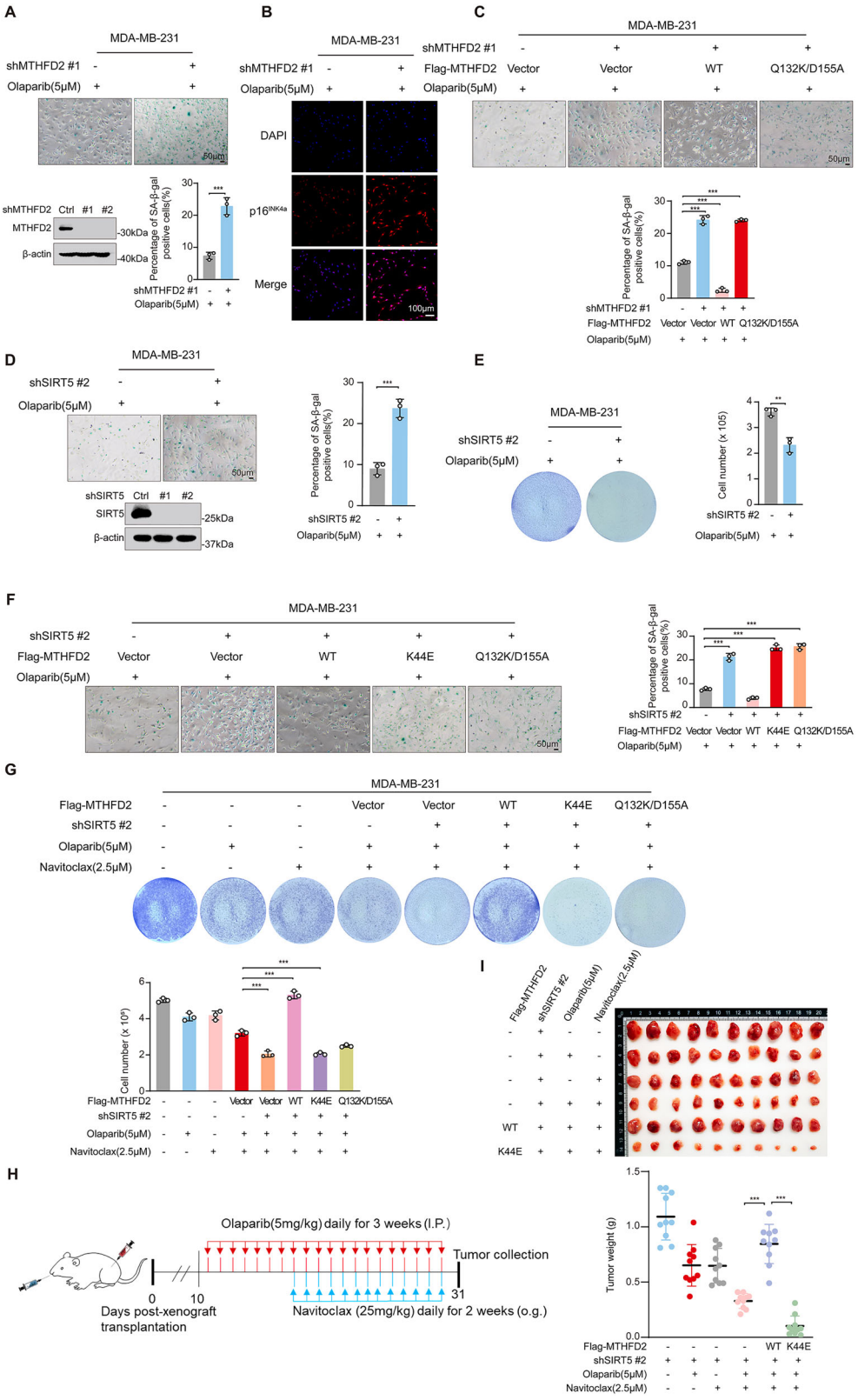

breast cancer cell senescence. TIS combined with senolytic treatment is a new strategy for tumor therapy in recent years[83]. In this study, we found that SIRT5-mediated desuccinylation can activate MTHFD2 activity, decrease TIS, and enhance chemoresistance in breast cancer cells. In vivo experiments confirmed that breast cancer cells with SIRT5 knockdown and high MTHFD2 succinylation were more sensitive to chemotherapeutic agents (olaparib). In conclusion, this study may imply that breast cancer cells with high levels of SIRT5 expression or high activity of MTHFD2 are less prone to TIS state during chemotherapy, which may be the main reason for the poorer prognosis of breast cancer patients, and the SIRT5-MTHFD2 axis is a potent metabolic target for regulating TIS or chemoresistance in breast cancer cells.

Fig. 7 | SIRT5-mediated desuccinylation of MTHFD2 enhances chemoresistance by reducing breast cancer sensitivity to TIS. A MDA-MB-231 cells were transfected with control or MTHFD2 shRNA#1, and treated with 5 μM Olaparib for 7 days, and cellular senescence was indicated by SA-β-gal staining. **B** MDA-MB-231 cells were transfected with control or MTHFD2 shRNA#1, and treated with 5 μM Olaparib for 7 days. The $p16^{INK4a}$ expression was detected by immunofluorescence. **C** MDA-MB-231 cells were transfected with control or MTHFD2 shRNA#1 in the presence of 3xFlag-MTHFD2-WT, 3xFlag-MTHFD2-K44E, and 3xFlag-Gln132Lys/Asp155Ala-MTHFD2, and treated with 5 μM Olaparib. The cellular senescence was indicated by SA-β-gal staining. **D** MDA-MB-231 cells were transfected with control or SIRT5 shRNA#2, and treated with 5 μM Olaparib for 7 days, and cellular senescence was indicated by SA-β-gal staining. **E** MDA-MB-231 cells were transfected with control or SIRT5 shRNA#2, and treated with 5 μM Olaparib for 7 days. The cell proliferation was assayed by crystal violet staining. **F** Effect of ectopic expression of WT MTHFD2, MTHFD2 K44E, and Gln132Lys/Asp155Ala-MTHFD2 mutant on TIS. MDA-MB-231 cells were transfected with shSIRT5#2 or shControl to knock out the endogenous SIRT5 and express FLAG-MTHFD2, FLAG-MTHFD2 K44E and Gln132Lys/Asp155Ala-MTHFD2, and then treated with 5 μM Olaparib for 7days. The cellular senescence was indicated by SA-β-gal staining. **G** MDA-MB-231 cells were transfected with control or SIRT5 shRNA#2 and overexpression WT MTHFD2, MTHFD2 K44E and Gln132Lys/Asp155Ala-MTHFD2 mutant, after a 6-day treatment with 5 μM Olaparib, cells were exposed to 2.5 μM Navitoclax combined with 5 μM Olaparib for 2 days. The cell proliferation was assayed by crystal violet staining. **H** BALB/c nude mice were orthotopically injected with MDA-MB-231 breast cancer cells and treated daily with either vehicle or Olaparib and Navitoclax. 2×10^6 MDA-MB-231 cells were subcutaneously implanted into the subcutaneous. When the tumor volume reached 60 mm^3, Olaparib (5mg/kg) treatment started and was maintained daily (i.p.) for 20 days. Navitoclax (25 mg/kg) treatments started 7 days after Olaparib treatment, and Navitoclax via oral gavage (o.g.) for 2 weeks. **I** Average images (up) and weights (down) of xenograft tumors (4 weeks, means ± S.D., $n = 5$) generated by SIRT5-silenced MDA-MB-231 cells and overexpressing 3xFlag-MTHFD2-WT or 3xFlag-MTHFD2-K44E as indicated. For all graphs, data are presented as mean ± SD, $^*p < 0.05$, $^{**}p < 0.01$, $^{***}p < 0.001$. Statistical analysis was performed with a paired *t* test.

Methods

Cell culture and treatments

U2OS, MDA-MB-231, MCF-7, MDA-MB-468, and MEF cells were purchased from the American Type Culture Collection (ATCC). HFF cells and IMR90 were presented by Fudan University. All cell lines were cultured in a 5% CO_2 humidified incubator (Thermo Fisher Scientific, Waltham, MA, USA) at 37 °C. U2OS, MDA-MB-231, MEF, IMR90, and HFF cell lines were routinely maintained in Dulbecco's modified Eagle's medium (DMEM) (Life Technologies, Carlsbad, CA). If not specified, all media were supplemented with 10% fetal bovine serum (FBS; Gemini). All cells were incubated in a culture medium without penicillin-streptomycin for less than two months and examined for mycoplasma annually.

Compounds were added at specific concentrations and times. For MG132 treatment, doses of 0.5 μM were used for 48-hour treatment. For Lys05 treatment, doses of 5 μM were used for 48-hour treatment. DES (20 mM), DMK (10 mM), 3-NPA (3 mM), and glycine (100 mM) were used to treat cells for 24 h. For TIS cell model, 50 μM ETOP for 48 hours or 100 μM H_2O_2 for 1 h.

Reagents and antibodies

Anti-Flag M2 magnetic beads (A2220) and NAM (S1899) were from Selleck. The NADPH (N5130), X-tremeGENE HP DNA Transfection Reagent (Roche, A06366236001) and succinyl CoA (S1129-5MG) were purchased from Sigma. DES (HY-44134), DMK (HY-Y0836), 3-NPA (HY-W012875) were purchased from MCE. 3×Flag peptides solution (P9801) was from Beyotime. The antibodies were commercially obtained: β-actin antibody (81115-1-RR, 1:5000), HA antibody (51064-2-AP, 1:5000), MTHFD2 antibody (12270-1-AP, 1:1000), SIRT5 antibody (15122-1-AP, 1:2000), p21(10355-1-AP, 1:1000) were from Proteintech. AMPKα (#2532, 1:1000), Phospho-AMPKα (Thr172) (#50081, 1:1000), p53(#9282, 1:1000), Phospho-p53 (Ser15) (#9284, 1:1000) were from Cell signaling technology. Flag antibody (M20008L, 1:3000) was from ABMART. Pan-succinylation antibody (PTM-0401, 1:1000) was from PTM BIO. The following reagents were purchased from Sigma-Aldrich: crystal violet (CV) and 0.4% trypan blue solution.

Plasmid construction

The pcDNA3.1-3xFlag-MTHFD2 and Myc-SIRT1-7 were purchased from You Bia. Point mutations in the MTHFD2 and SIRT5 constructs were generated using a Site-Directed Mutagenesis kit (#E0552S) purchased from novel England Biolabs. Myc-SIRT5-SIRT5Δ50 was purchased from GenePharma. Lipofectamine 2000 (Invitrogen) was used for cell transfection assays.

siRNA or shRNA

The siRNAs used in this study were synthesized by Gene Pharma (Shanghai, China). The sequences for targeting SIRT5 and MTHFD2 are listed in Supplementary information files (Supplementary Table 1). Lipofectamine RNAiMAX transfection agent (Invitrogen, Carlsbad, CA, USA) was used to transfect cells with siRNAs (20 nM). The shRNA sequences for MTHFD2 and SIRT5 were cloned into pLKO.1 TRC (Addgene plasmid 10879) and verified by DNA sequencing. Once introduced, the puromycin resistance marker encoded in pLKO.1 allows for convenient, stable selection. The shRNA sequences are listed in Supplementary information files (Supplementary Table 1). Lipofectamine 2000 (Invitrogen) was used for cell transfection assays.

Quantitative RT-PCR analysis

Total RNA was isolated from the cells using an RNA extraction kit (DAKEWE, Cat# 8034111). Then, the First-strand cDNA Synthesis System (Thermo Scientific ReverAid First Strand cDNA Synthesis Kit, Cat# K1622) was used to reverse transcribe cDNA from RNA (1 μg). Subsequently, cDNA (0.2 μg) was used as a template and was amplified by quantitative PCR with specific primer sequences. Quantitative PCR amplification was performed using SYBR Green PCR Master Mix (Genestar, Cat# A308). The primer sequences used for different genes are listed in Supplementary information files (Supplementary Table 2).

Mass spectrometry and LC-MS/MS analysis

The tryptic peptides, meticulously dissolved in solvent A, were directly loaded onto a homemade reversed-phase analytical column (25 cm length, 100 μm i.d.). The mobile phase, a carefully balanced mixture of solvent A (0.1% formic acid, 2% acetonitrile/in water) and solvent B (0.1% formic acid in acetonitrile), facilitated the separation of peptides. This separation was executed with a precise gradient: 0–18 min, 6–22%B ; 18–22 min, 22–30% B ; 22–26 min, 30–80%B ; 26–30 min, 80%B, all at a constant flow rate of 450 nl/min on a NanoElute UHPLC system (Bruker Daltonics). The peptides then underwent capillary source and timsTOF Pro mass spectrometry, with an electrospray voltage of 1.6 kV. The timsTOF Pro operated in data independent parallel accumulation serial fragmentation (dia-PASEF) mode, with a full MS scan set as100-1700 (MS/MS scan range) and 8PASEF (MS/MS mode)-MS/MS scans acquired per cycle. The MS/MS scan range was set as 425–1025 and the isolation window was set as25 *m/z*, ensuring the precision of the entire process.

Building the Spectral Library: The DDA data were meticulously processed using Spectronaut (v.18) software coupled with the Pulsar search engine. Tandem mass spectra were exhaustively searched against the Homo_sapiens_9606_SP_20231220.fasta (20429 entries) concatenated with a reverse decoy database. The max missing cleavages were set as 2, and specific modifications were carefully specified. The false discovery rate (FDR) of protein, peptide, and PSM was rigorously adjusted to <1%, ensuring the thoroughness of the analysis. The resulting spectral library, imported into Spectronaut (v.18) software, was used to predict the retention

time by nonlinear correction and searched against DIA data, further validating the results.

Bioinformatics analyses

The process of GO annotation involves using the eggnog-mapper software to extract GO IDs from the identified proteins based on the EggNOG database and then performing functional classification annotation analysis on the proteins according to cellular components, molecular functions, and biological processes.

The structural domain of a protein is a specific protein region that is conserved in sequence and can generally perform a function independently. It is also a structural component of molecular function, generally consisting of 25 to 500 amino acids. These areas are relatively spatially compact, structurally stable, and capable of being independently folded into functional structures. A protein may have multiple domains, and a domain may also exist in multiple proteins. In the project data, protein structural domain annotation was performed on the identified proteins based on the Pfam database and the corresponding PfamScan tool. We annotate protein pathways based on the KEGG pathway database and identify proteins through BLAST comparison (blastp, value ≤ 1e−4); for each sequence, the annotation is based on the top-scoring comparison result.

Western blot Analysis

Whole-cell lysates were prepared in modified RIPA lysis buffer (10 mM Tris–HCl pH 7.5, 5 mM EDTA, 150 mM NaCl, 1% NP-40, 1% sodium deoxycholate, 0.025% SDS, and complete protease cocktail). Cells were washed, incubated in lysis buffer for 30 min on ice, and boiled in 5x loading buffer. Protein samples were resolved by SDS-PAGE and transferred onto a nitrocellulose membrane. The membrane was blocked with 5% skim milk in TBST and probed with the indicated antibodies.

Co-immunoprecipitation (Co-IP)

Cells were lysed in NP40 lysis buffer (50 mM Tris-HCl, pH 7.5, 150 mM NaCl, 0.1%–0.5% NP40, 1 mM PMSF, and related protease inhibitors). Co-IP assays were performed by incubating anti-Flag M2 magnetic beads (A2220, Sigma, USA) at 4° C for over 4 h. After incubation, the beads were washed three times with ice-cold NP40 buffer, and the proteins were eluted in 1×loading buffer by heating at 100° C for 10 min. Finally, the eluted proteins were analyzed by western blotting.

MTHFD2 enzyme activity

MTHFD2 protein immunoprecipitated from cells and substrate were added to detection buffer (50 mM Tris–HCl, 30 mM β-mercaptoethanol, 5 mM $MgCl_2$, 1 mM NAD, pH 8.0). The mixture was incubated at 30° C for 2 min and stopped by 1 M HCl. The absorbance was measured at 350 nm and the final result was obtained by normalization with the quantified protein concentration. Data on enzyme activities were from at least triplicate wells.

NADPH transfection

For NADPH transfection in IMR90 and HFF, cells were seeded into a six-well dish. 40%–50% confluent cells were changed with fresh DMEM containing 10% CS. Before transfection, 10 μM NADPH was diluted with 200 μl Opti-MEM in a sterile tube and mixed gently. Afterwards, 5 μl X-tremeGENE HP DNA Transfection Reagent was pipetted into the tube. The transfection complex was mixed and then added into cells in a dropwise manner (incubated for 15-30 min at room temperature).

NADPH and ROS levels

NADPH levels and $NADP^+$/NADPH ratios were determined using a $NADP^+$/NADPH quantification kit (BioVision, Mountain View, CA, USA, catalog no: K347). The reactive oxygen species levels were determined: The cells were incubated at 37° C for 30 min in PBS containing 2', 7'-dichlorodihydrofluorescein diacetate (DCFH-DA, 10 μM). The cells were washed twice with PBS, treated with trypsin, and resuspended in PBS. Fluorescence was measured immediately using a flow cytometer (Wellgrow, Shenzhen, China).

Cell proliferation assay

MDA-MB-231 cells were transfected with siRNAs for 48 h, seeded in 6-well cell culture dishes at a density of 20,000 cells/well, and then supplemented with or without 40 μM olaparib. The cell number at a specified time point was recorded using a hemocytometer. For the crystal violet (CV) staining assay, the cells were fixed with 10% formalin for 10 min and stained with 0.05% CV for 10 min. The cells were washed with distilled water and imaged.

Senescence-associated β-galactosidase (SA-β-gal) staining

The SA-β-gal activity of HFF was measured by the Senescence β-Galactosidase Staining Kit (Cell Signaling Technology, #9860 s). Cells were cultured in 6-well plates, washed with PBS, and fixed for 10-15 min at room temperature. Cells were washed twice with PBS and incubated with the staining mixture at 37° C overnight. The SA-β-gal signals were analyzed using Image Pro Plus. For each staining assay, the late passage (P30) or H_2O_2-treated HFF was used as the positive control, while the early passage (P10) HFF was used as the negative control.

Senescence induction models

For RS: Primary human foreskin fibroblasts (HFFs) were obtained from the American Type Culture Collection (ATCC) and cultured in Dulbecco's Modified Eagle Medium (DMEM) supplemented with 15% fetal bovine serum (FBS). In our experimental system, cells were passaged at a ratio of 1:3 when they reached approximately 80–90% confluency in T25 flasks. This typically occurred every 3–4 days. The passage number was incremented by one with each split (denoted as Pn+1). For example, "P10" refers to cells that have undergone ten consecutive passages since initial seeding. For OIS: Viral particles were generated by transfecting HEK293T cells grown in 10-cm dishes with 8 μg of total DNA, including ER: RAS plasmid, VSVG, and packaging plasmid (LECO), using Lipofectamine 2000. Six hours post-transfection, the medium was replaced with fresh complete medium. Viral supernatants were harvested 48–72 h later and filtered through a 0.45 μm syringe filter. P18 HFF or early-passage IMR90 cells (50–60% confluency) were infected with the filtered viral supernatant diluted in growth medium. After 48–72 h of infection, cells were selected with G418 (300 μg/mL) until control cells died. To induce ER: RAS expression, selected cells were treated with 4-hydroxytamoxifen (4-OHT, final concentration: 100 μM) in complete medium. Senescence phenotypes typically developed 7–10 days after induction. For CIS induction: early-passage HFF or IMR90 cells were treated with 50 μM etoposide for 48 hours. Following treatment, cells were washed thoroughly with PBS and cultured in fresh complete medium for an additional 3 days to allow the senescence phenotype to fully develop. For Oxidative Stress-Induced Senescence (OSIS): Oxidative stress-induced premature senescence was established by exposing early-passage HFF or IMR90 cells to 100 μM hydrogen peroxide (H_2O_2) for 1 hour at 37° C. Cells were then washed and maintained in fresh complete medium for 3–5 days prior to analysis.

Xenograft tumor models

All mice were treated in strict accordance with the ethical guidelines and protocols approved by Inner Mongolia University (IMU-MOUSE-2024-084). We have complied with all relevant ethical regulations for animal use. All mice used in this study were 4-week-old male athymic Balb-c mice. All mice were maintained in ventilated cages within a specific pathogen-free animal facility. 2×10^6 MDA-MB-231 breast cancer cells (shControl/3xFlag-WT, shMTHFD2/3xFlag-WT, and shMTHFD2/3xFlag-K44E) were injected subcutaneously into the flanks of 4-week-old athymic Balb-c male mice. Tumors were measured with callipers every 2 days, and the tumor volume (mm^3) was calculated with the formula length × $width^2/2$. When tumor volume reached an average of 100 mm^3, olaparib (5 mg/kg) were intraperitoneally injected by once a day for 2 weeks.

For assays testing the combination of olaparib and Navitoclax treatment. 2×10^6 MDA-MB-231 breast cancer cells (shSIRT5/3xFlag-Vector, shSIRT5/3xFlag-WT, shSIRT5/3xFlag-K44E) were injected subcutaneously into the flanks of 4-week-old athymic Balb-c male mice. When tumor volume reached an average of 60mm3, olaparib (5mg/kg) was intraperitoneally injected three times/week for 2 weeks. The day after the initiation of olaparib treatment, Navitoclax (50 mg/kg) is administered via oral gavage for 6 consecutive days in two cycles.

Data analysis on public datasets

Box plot analysis of MTHFD2 expressions in normal tissue versus tumors was generated from the TCGA dataset (https://portal.gdc.com). Correlation plots of SIRT5 MTHFD2 expression in the BRCA dataset ($n = 1100$ patients) were downloaded from TCGA. RNA-sequencing expression (level 3) profiles and corresponding clinical information for 1100 BRCA were downloaded from the TCGA dataset (https://portal.gdc.com). Data were presented using the log2 scale, and the Spearman correlation coefficient was used. Spearman's correlation analysis describes the correlation between quantitative variables without a normal distribution. *P-values* less than 0.05 were considered statistically significant. Kaplan-Meier survival analysis of the gene signature from the TCGA dataset with BRCA、SARC、UCEC, and LUAD based on MTHFD2 expression. The Affyid/Gene symbol we used in this online database is as follows: MTHFD2 (201761_at).

Statistics and reproducibility

All experiments were performed at least three times, and results were presented as the means ± SD. To determine the significance between the tested groups, a paired *t* test analysis was performed with Prism 8. $^*P < 0.05$, $^{**}P < 0.01$, $^{***}P < 0.001$, ns = insignificant. $P < 0.05$ was considered statistically significant.

Reporting summary

Further information on research design is available in the Nature Portfolio Reporting Summary linked to this article.

Data availability

All data generated or analyzed during this study are included in this published article (and its supplementary information files). Raw proteomics data generated by 4D-FastDIA for quantification of succinylation modifications in U2OS cell samples are available in Supplementary Data 1. The source data for graphs are provided in Supplementary Data 2. Full blots are shown in Supplementary information files (Supplementary Fig. 5). All data generated or analyzed during this study are available from the corresponding author on reasonable request. The mass spectrometry data have been deposited to the Proteome X change Consortium via the iPro X partner repository with the dataset identifier PXD029909. URL, https://www.iprox.cn/page/DSV021.html;?url=175868183295053C9I, Password: 5Kmb.

Received: 18 February 2025; Accepted: 11 September 2025;
Published online: 20 October 2025

References

1. Wilkinson, L. & Gathani, T. Understanding breast cancer as a global health concern. *Br. J. Radiol.* **95**, 20211033 (2022).
2. Marquette, C. & Nabell, L. Chemotherapy-resistant metastatic breast cancer. *Curr. Treat. Options Oncol.* **13**, 263–275 (2012).
3. Trapani, D. et al. Global challenges and policy solutions in breast cancer control. *Cancer Treat. Rev.* **104**, 102339 (2022).
4. Litwiniec, A. et al. Low-dose etoposide-treatment induces endoreplication and cell death accompanied by cytoskeletal alterations in A549 cells: Does the response involve senescence? The possible role of vimentin. *Cancer Cell Int.* **13**, 9 (2013).
5. Ewald, J. A. et al. Therapy-induced senescence in cancer. *J. Natl Cancer Inst.* **102**, 1536–1546 (2010).
6. Saleh, T. et al. Therapy-induced senescence as a component of tumor biology: Evidence from clinical cancer. *Biochim. Biophys. Acta Rev. Cancer* **1878**, 188994 (2023).
7. Li, F. et al. Blocking methionine catabolism induces senescence and confers vulnerability to GSK3 inhibition in liver cancer. *Nat. Cancer* **5**, 131–146 (2024).
8. Tolsma, T. O. & Hansen, J. C. Post-translational modifications and chromatin dynamics. *Essays Biochem.* **63**, 89–96 (2019).
9. Zhang, Z. et al. Identification of lysine succinylation as a new post-translational modification. *Nat. Chem. Biol.* **7**, 58–63 (2011).
10. Zhang, N. et al. Cholangiocarcinoma PDHA1 succinylation suppresses macrophage antigen presentation via alpha-ketoglutaric acid accumulation. *Nat. Commun.* **16**, 3177 (2025).
11. Zhang, Y. et al. Lysine desuccinylase SIRT5 binds to cardiolipin and regulates the electron transport chain. *J. Biol. Chem.* **292**, 10239–10249 (2017).
12. Yang, S. et al. HIF1α/ATF3 partake in PGK1 K191/K192 succinylation by modulating P4HA1/succinate signaling in glioblastoma. *Neuro-Oncol.* **26**, 1405–1420 (2024).
13. Wu, M. et al. Sirt5 improves cardiomyocytes fatty acid metabolism and ameliorates cardiac lipotoxicity in diabetic cardiomyopathy via CPT2 de-succinylation. *Redox Biol.* **73**, 103184 (2024).
14. Zhang, R. et al. Regulation of urea cycle by reversible high-stoichiometry lysine succinylation. *Nat. Metab.* **6**, 550–566 (2024).
15. Liang, L. et al. Alterations in PD-L1 succinylation shape anti-tumor immune responses in melanoma. *Nat. Genet.* **57**, 680–693 (2025).
16. Lu, S. et al. Succinate-loaded tumor cell-derived microparticles reprogram tumor-associated macrophage metabolism. *Sci. Transl. Med.* **17**, eadr4458 (2025).
17. Peng, C. et al. The first identification of lysine malonylation substrates and its regulatory enzyme. *Mol. Cell. Proteomics* **10** M111.012658 (2011).
18. Zhao, Q. et al. SIRT5 safeguards against primate skeletal muscle ageing via desuccinylation of TBK1. *Nat. Metab.* **7**, 556–573 (2025).
19. Sun, R. et al. Loss of SIRT5 promotes bile acid-induced immunosuppressive microenvironment and hepatocarcinogenesis. *J. Hepatol.* **77**, 453–466 (2022).
20. Chen, X.-F. et al. SIRT5 inhibits peroxisomal ACOX1 to prevent oxidative damage and is downregulated in liver cancer. EMBO Rep. **19**, (2018).
21. Wang, H.-L. et al. Sirtuin5 protects colorectal cancer from DNA damage by keeping nucleotide availability. *Nat. Commun.* **13**, 6121 (2022).
22. Abril, Y. L. N. et al. Pharmacological and genetic perturbation establish SIRT5 as a promising target in breast cancer. *Oncogene* **40**, 1644–1658 (2021).
23. Finley, L. W. S. What is cancer metabolism?. *Cell* **186**, 1670–1688 (2023).
24. Shin, M., Momb, J. & Appling, D. R. Human mitochondrial MTHFD2 is a dual redox cofactor-specific methylenetetrahydrofolate dehydrogenase/methenyltetrahydrofolate cyclohydrolase. *Cancer Metab.* **5**, 11 (2017).
25. Yue, L. et al. Mthfd2 modulates mitochondrial function and DNA repair to maintain the pluripotency of mouse stem cells. *Stem Cell Rep.* **15**, 529–545 (2020).
26. Yang, Y. & Gibson, G. E. Succinylation links metabolism to protein functions. *Neurochem. Res.* **44**, 2346–2359 (2019).
27. Rather, G. M. et al. In cancer, all roads lead to NADPH. *Pharmacol. Therapeutics* **226**, 107864 (2021).
28. Reczek, C. R. et al. A CRISPR screen identifies a pathway required for paraquat-induced cell death. *Nat. Chem. Biol.* **13**, 1274–1279 (2017).
29. Dodson, M., Castro-Portuguez, R. & Zhang, D. D. NRF2 plays a critical role in mitigating lipid peroxidation and ferroptosis. *Redox Biol.* **23**, 101107 (2019).

30. Ju, H.-Q. et al. NADPH homeostasis in cancer: functions, mechanisms and therapeutic implications. *Signal Transduct. Target. Ther.* **5**, 231 (2020).
31. Ilter, D. et al. NADK-mediated de novo NADP(H) synthesis is a metabolic adaptation essential for breast cancer metastasis. *Redox Biol.* **61**, 102627 (2023).
32. Li, M. et al. Aldolase B suppresses hepatocellular carcinogenesis by inhibiting G6PD and pentose phosphate pathways. *Nat. Cancer* **1**, 735–747 (2020).
33. Jiang, P. et al. Reciprocal regulation of p53 and malic enzymes modulates metabolism and senescence. *Nature* **493**, 689–693 (2013).
34. Pirozzi, C. J. & Yan, H. The implications of IDH mutations for cancer development and therapy. *Nat. Rev. Clin. Oncol.* **18**, 645–661 (2021).
35. Liu, X.-L., Ding, J. & Meng, L.-H. Oncogene-induced senescence: a double edged sword in cancer. *Acta Pharmacologica Sin.* **39**, 1553–1558 (2018).
36. Chen, H. et al. NBS1 lactylation is required for efficient DNA repair and chemotherapy resistance. *Nature* **631**, 663–669 (2024).
37. Zhang, J. et al. PARylated PDHE1α generates acetyl-CoA for local chromatin acetylation and DNA damage repair. *Nat. Struct. Mol. Biol.* **30**, 1719–1734 (2023).
38. Chen, Y. et al. Metabolic regulation of homologous recombination repair by MRE11 lactylation. *Cell* **187**, (2024).
39. Shen, R. et al. Lysine succinylation, the metabolic bridge between cancer and immunity. *Genes Dis.* **10**, 2470–2478 (2023).
40. Gao, X. et al. Systematic analysis of lysine acetylome and succinylome reveals the correlation between modification of H2A.X complexes and DNA damage response in breast cancer. *Oncol. Rep.* **43**, 1819–1830 (2020).
41. Vasan, K., Werner, M. & Chandel, N. S. Mitochondrial metabolism as a target for cancer therapy. *Cell Metab.* **32**, 341–352 (2020).
42. Zhou, L. et al. SIRT5 promotes IDH2 desuccinylation and G6PD deglutarylation to enhance cellular antioxidant defense. *EMBO Rep.* **17**, 811–822 (2016).
43. Teng, P. et al. SIRT5-mediated ME2 desuccinylation promotes cancer growth by enhancing mitochondrial respiration. *Cell Death Differ.* **31**, 65–77 (2024).
44. Scallet, A. C. et al. 3-nitropropionic acid inhibition of succinate dehydrogenase (complex II) activity in cultured Chinese hamster ovary cells: antagonism by L-carnitine. *Ann. N. Y. Acad. Sci.* **993**, (2003).
45. Li, F. et al. NADP(+)-IDH mutations promote hypersuccinylation that impairs mitochondria respiration and induces apoptosis resistance. *Mol. Cell* **60**, 661–675 (2015).
46. Sugiura, A. et al. MTHFD2 is a metabolic checkpoint controlling effector and regulatory T cell fate and function. *Immunity* **55**, (2022).
47. Zhao, R. et al. PPFIA4 promotes castration-resistant prostate cancer by enhancing mitochondrial metabolism through MTHFD2. *J. Exp. Clin. Cancer Res. : CR* **41**, 125 (2022).
48. Amaravadi, R. K. & Winkler, J. D. Lys05: a new lysosomal autophagy inhibitor. *Autophagy* **8**, 1383–1384 (2012).
49. Dou, Z. et al. Autophagy mediates degradation of nuclear lamina. *Nature* **527**, 105–109 (2015).
50. Cheng, X.-T. et al. Revisiting LAMP1 as a marker for degradative autophagy-lysosomal organelles in the nervous system. *Autophagy* **14**, 1472–1474 (2018).
51. Sena, L. A. & Chandel, N. S. Physiological roles of mitochondrial reactive oxygen species. *Mol. Cell* **48**, 158–167 (2012).
52. Shadel, G. S. & Horvath, T. L. Mitochondrial ROS signaling in organismal homeostasis. *Cell* **163**, 560–569 (2015).
53. Warraich, U.-E. A., Hussain, F. & Kayani, H. U. R. Aging-oxidative stress, antioxidants and computational modeling. *Heliyon* **6**, e04107 (2020).
54. Di Meo, S. et al. Role of ROS and RNS sources in physiological and pathological conditions. *Oxid. Med. Cell. Longev.* **2016**, 1245049 (2016).
55. Guo, Y. et al. Mitochondrial dysfunction in aging. *Ageing Res. Rev.* **88**, 101955 (2023).
56. Vousden, K. H. & Prives, C. Blinded by the light: the growing complexity of p53. Cell **137**, 413–431 (2009).
57. Ben-Porath, I. & Weinberg, R. A. The signals and pathways activating cellular senescence. *Int. J. Biochem. Cell Biol.* **37**, 961–976 (2005).
58. Ju, H.-Q. et al. Modulation of redox homeostasis by inhibition of MTHFD2 in colorectal cancer: mechanisms and therapeutic implications. *J. Natl Cancer Inst.* **111**, 584–596 (2019).
59. Lin, S.-C. & Hardie, D. G. AMPK: sensing glucose as well as cellular energy status. *Cell Metab.* **27**, 299–313 (2018).
60. Blättler, S. M. et al. In the regulation of cytochrome P450 genes, phenobarbital targets LKB1 for necessary activation of AMP-activated protein kinase. *Proc. Natl Acad. Sci. USA* **104**, 1045–1050 (2007).
61. Covarrubias, A. J. et al. Senescent cells promote tissue NAD+ decline during ageing via the activation of CD38+ macrophages. *Nat. Metab.* **2**, 1265–1283 (2020).
62. Wu, Q.-J. et al. The sirtuin family in health and disease. *Signal Transduct. Target. Ther.* **7**, 402 (2022).
63. Bi, S. et al. The sirtuin-associated human senescence program converges on the activation of placenta-specific gene PAPPA. *Dev. Cell* **59**, (2024).
64. Caetano-Pinto, P. et al. The importance of breast cancer resistance protein to the kidneys excretory function and chemotherapeutic resistance. *Drug Resist. Updat.* **30**, 15–27 (2017).
65. Wang, L. et al. cFLIP suppression and DR5 activation sensitize senescent cancer cells to senolysis. *Nat. Cancer* **3**, 1284–1299 (2022).
66. Estepa-Fernández, A. et al. Combination of palbociclib with navitoclax based-therapies enhances in vivo antitumoral activity in triple-negative breast cancer. *Pharmacol. Res.* **187**, 106628 (2023).
67. Jarrold, J. & Davies, C. C. PRMTs and arginine methylation: cancer's best-kept secret? *Trends Mol. Med.* **25**, (2019).
68. Goldstein, M. & Kastan, M. B. The DNA damage response: implications for tumor responses to radiation and chemotherapy. *Annu. Rev. Med.* **66**, 129–143 (2015).
69. Li, G. et al. Glycometabolic reprogramming-induced XRCC1 lactylation confers therapeutic resistance in ALDH1A3-overexpressing glioblastoma. Cell Metabolism, **36**, (2024).
70. Li, X. et al. Deacetylation induced nuclear condensation of HP1γ promotes multiple myeloma drug resistance. *Nat. Commun.* **14**, 1290 (2023).
71. He, C. et al. SOD2 acetylation on lysine 68 promotes stem cell reprogramming in breast cancer. *Proc. Natl Acad. Sci. USA* **116**, 23534–23541 (2019).
72. Wang, X. et al. Succinylation inhibits the enzymatic hydrolysis of the extracellular matrix protein fibrillin 1 and promotes gastric cancer progression. *Adv. Sci. (Weinh., Baden.-Wurtt., Ger.)* **9**, e2200546 (2022).
73. Qi, H. et al. Succinylation-dependent mitochondrial translocation of PKM2 promotes cell survival in response to nutritional stress. *Cell Death Dis.* **10**, 170 (2019).
74. Yang, Y. et al. Mitochondria and mitochondrial ROS in cancer: novel targets for anticancer therapy. *J. Cell. Physiol.* **231**, 2570–2581 (2016).
75. Liu, Y. E. et al. The diversified role of mitochondria in ferroptosis in cancer. *Cell Death Dis.* **14**, 519 (2023).
76. Wang, Y. et al. The double-edged roles of ROS in cancer prevention and therapy. *Theranostics* **11**, 4839–4857 (2021).
77. Fernández, ÁF. et al. Disruption of the beclin 1-BCL2 autophagy regulatory complex promotes longevity in mice. *Nature* **558**, 136–140 (2018).

78. Sreedhar, A., Wiese, E. K. & Hitosugi, T. Enzymatic and metabolic regulation of lysine succinylation. *Genes Dis.* **7**, 166–171 (2020).
79. Kida, Y. & Goligorsky, M. S. Sirtuins, cell senescence, and vascular aging. *Can. J. Cardiol.* **32**, 634–641 (2016).
80. Wang, Y.-Q. et al. Sirtuin5 contributes to colorectal carcinogenesis by enhancing glutaminolysis in a deglutarylation-dependent manner. *Nat. Commun.* **9**, 545 (2018).
81. Liu, X. et al. Repression of p53 function by SIRT5-mediated desuccinylation at Lysine 120 in response to DNA damage. *Cell Death Differ.* **29**, 722–736 (2022).
82. Yang, X. et al. SHMT2 desuccinylation by SIRT5 drives cancer cell proliferation. *Cancer Res.* **78**, 372–386 (2018).
83. Schmitt, C. A., Wang, B. & Demaria, M. Senescence and cancer—role and therapeutic opportunities. *Nat. Rev. Clin. Oncol.* **19**, 619–636 (2022).

Acknowledgements

This work was supported by the the National Natural Science Foundation of China (grant numbers 32400618), the Neimenggu Natural Science Foundation Project (2024QN03005) awarded to the Shuailin Hao, the National Natural Science Foundation of China (grant numbers 92249302, 32370592) awarded to T.N., and the State Key Laboratory of Reproductive Regulation & Breeding of Grassland Livestock (Grant number 2025KYPT0081).

Author contributions

T.N., S.H., X.Z., and Y.G. designed the experiments. Y.D., X.Z., Y.G., YC.Z., Y.C., X.P., J.Z. Y.Z., and Y.W. performed experiments. X.Z. and Y.G. analyzed the data. X.Z. and Y.G. reviewed the data and made substantial contributions to improving the studies. X.Z. and Y.G. wrote the manuscript, which was reviewed by all authors.

Competing interests

The authors declare no competing interests.

Additional information

Supplementary information The online version contains supplementary material available at https://doi.org/10.1038/s42003-025-08878-z.

Correspondence and requests for materials should be addressed to Du Yitian, Hao Shuailin or Ni Ting.

Peer review information *Communications Biology* thanks the anonymous reviewers for their contribution to the peer review of this work. Primary Handling Editors: Marina Holz and Kaliya Georgieva. A peer review file is available.